

Clues to the nature of damped Lyman alpha systems from chemical evolution models

Gustavo A. Lanfranchi¹ and Amancio C. S. Friça¹

¹*IAG-USP, R. do Matão 1226, Cidade Universitária, 05508-900 São Paulo, SP, Brazil*

25 October 2018

ABSTRACT

The evolution of the metallicity of damped Lyman α systems (DLAs) is investigated in order to explore several scenarios for the nature of these systems. The observational data on chemical abundances of DLAs are analysed with robust statistical methods, and the abundances are corrected for dust depletion. The results of this analysis are compared to predictions of several classes of chemical evolution models describing a variety of scenarios for DLAs: one-zone dwarf galaxy models, multi-zone disk models, and chemodynamical models representing dwarf galaxies. In order to settle constraints for star formation time scales and metal production in DLAs, we compare the observational data on the $[\alpha/\text{Fe}]$ and $[\text{N}/\alpha]$ ratios to the predictions from the models. In DLAs, these ratios are only partially reproduced by the dwarf galaxy one-zone model and by the disk model. On the other hand, the chemodynamical model for dwarf galaxies reproduces the properties of nearly all DLAs. The connection between the gas flow evolution and the star formation rate is the reason for the ability of this model in reproducing the range of abundance ratios seen in DLAs. The comparison of the observed $[\alpha/\text{Fe}]$ and $[\text{N}/\alpha]$ trends to the predictions of the chemodynamical model is used to derive the formation epoch of dwarf galaxies. The chemodynamical model predicts that dwarf galaxies make a significant contribution to the observed total neutral gas density in DLAs, and that this contribution is more important at high redshifts ($z \gtrsim 2 - 3$). This is consistent with a scenario in which the DLA population is dominated by dwarf galaxies at high redshifts and by disks at lower redshifts. The relation between DLAs and Lyman Break Galaxies (LBGs) is investigated with chemodynamical models describing LBGs. Our results call for a smoother progression in the evolutionary history of DLAs and LBGs rather than a sharp dichotomy between the two populations. LBGs and DLAs may constitute a sequence of increasing star formation rate, with the LBGs being systems with typically short star formation time scales ($\sim 10^8$ yr), and the DLAs having slower star formation. We also arise the possibility that we could be missing a whole population of high HI density column objects, with metallicities intermediate between those of DLAs and LBGs. Finally, we discuss the possibility that relying only on the observations of DLAs could lead to an underestimate of the metal content of the high redshift Universe.

Key words: cosmology: observations – galaxies: evolution – galaxies: formation – galaxies: ISM – intergalactic medium – quasars: general

1 INTRODUCTION

The study of chemical abundances in the QSO absorption line systems (QALs) and their evolution with redshift are key factors to be considered in our attempts to track the history of galaxy formation in the Universe. These systems are also essential in tracing the cosmic chemical evolution because they sample a variety of environments and are rep-

resentative systems of the early Universe, being enriched by the first stellar generations (Pettini et al. 1997a, 2000a).

The Damped Lyman α Systems (DLAs) are the QALs with the highest neutral hydrogen column densities ($N(\text{HI}) \gtrsim 10^{20} \text{ cm}^{-2}$). These systems are considered to be the most suitable for chemical abundance studies in the high-redshift Universe because they are believed to be the progenitors of present day galaxies, for a number of reasons. Owing to

their very large N(HI) values the DLAs dominate the neutral content of the universe (Wolfe et al. 1995; Rao & Turnshek 2000). Furthermore, the comoving baryonic mass density in gas inferred from the DLAs at $z = 2 - 3$ nearly coincides with the current baryonic mass density in stars today (Wolfe et al. 1995; Storrie-Lombardi & Wolfe 2000).

The high density column of these systems allowed abundance measurements of a number of elements never detected before in QALs, as is the case of zinc, which has an important role in DLA studies (on the other hand, strong lines of abundant elements, e.g. oxygen, become saturated, making it difficult to measure their abundances). In addition, their large N(HI) values require little ionization corrections (Viegas 1995, Vladilo et al. 2001). In the last few years, accurate abundances of several chemical elements have been derived for DLAs at high z (Lu et al. 1996, Prochaska & Wolfe 1999, Prochaska et al. 2001, Centurión et al. 2000, Molaro et al 2001), allowing detailed studies of chemical evolution in these systems, even though there are uncertainties that must be taken into account, such as depletion of some refractory elements onto dust grains and selection effects.

A widespread indicator of the metallicity in DLAs is the Zn abundance ($[Zn/H]$), which is believed to be very little or not affected at all by dust depletion. The Zn abundances range from -2 to 0 (Vladilo 1998, Lauroesch et al. 1996, Pettini et al. 1994, 1997b), suggesting that DLAs have a range of formation epochs or star formation histories. The form of the evolution of metallicity with redshift is not yet clearly known. Several studies argue that at $z < 2$ the mean metallicity of damped systems is approximately 1/10 - 1/30 solar with a large scatter and that it decreases at $z \approx 3$, even though the picture here is less certain (Pettini et al. 1994, Pettini et al 1997b, Pettini 1999, Lu et al. 1996, Prochaska & Wolfe 1999). By contrast, in a more extended work, Prochaska & Wolfe (2002) concluded that there is no significant evolution in metallicity of the DLAs over the $z \approx 1.5 - 3.5$ range, although there appears to be a marked decline at $z > 3.5$, but only by a factor of a few.

Abundance ratios would be a better tool in DLAs chemical evolution studies. Unlike absolute values, abundance ratios do not strongly depend on particular model parameters, but mainly on the stellar nucleosynthesis and the adopted IMF. The $[\alpha/Fe]$ and $[N/\alpha]$ ratios can be used to settle constraints on time scales for star formation and metal production. While the α elements are mainly produced in type II Supernovae (SNe II) in short time scales, the Fe-peak elements are produced in type Ia Supernovae (SNe Ia) in a longer time scale. A slow (long time scale) star formation correspond to nearly solar values of $[\alpha/Fe]$ while supra-solar values may indicate shorter time scales for the star formation, which is dominated by SNe II. The $[N/\alpha]$ ratio can also indicate the star formation time scale, because the ejection of nitrogen (mainly produced in intermediate mass stars) into the interstellar medium (ISM) is delayed with respect to that of the α elements. There is a controversy, though, about the observed pattern of the $[\alpha/Fe]$ ratio in DLAs. Some authors (Pettini et al. 2000a, Ellison et al. 2001a) detect an $[\alpha/Fe]$ enhancement similar to that of the metal-poor stars of our Galaxy, although the enhancement levels are typically lower in DLAs. In contrast, other works find nearly solar $[\alpha/Fe]$ ratios, as expected from the chemical

evolution of dwarf galaxies (Centurión et al. 2000, Molaro et al. 2001).

The discrepancy between the values of the $[\alpha/Fe]$ ratio determined by different authors may be related to the way they consider dust depletion. It has long been realized that dust depletion is a major problem concerning the chemical evolution of DLAs, because the observed abundances probe only the gas phase of the DLA ISM. Pettini et al. (1994) demonstrated that the majority of DLAs exhibit an enhancement of Zn relative to Cr, which they interpreted as evidence of dust depletion. In addition, DLA surveys generally use QSOs selected from magnitude limited samples, in which QSOs that lie behind dusty, and presumably metal-rich DLAs would be under-represented (Pei & Fall 1995). One must know the depletion fraction of each element in each system in order to determine its real abundance pattern; the observed abundance refers only to the fraction of the element in gaseous form. Several authors have proposed different approaches to this problem, but there is not yet consensus about the procedure to correct for dust depletion. Pettini et al. (2000a) applied an uniform dust depletion correction to refractory elements in systems for which dust/gas ratio is less than 50 %. Savaglio et al. (1999) compared the DLAs depletion patterns to those of our own Galaxy in order to elaborate a correction for each system separately. Vladilo (1998, 2002b), on the other hand, suggested more elaborated methods for dust correction based on the dust chemical composition and intrinsic abundances of two elements (Zn and Fe) with different dust depletion properties. Previous works (Vladilo 1998) assumed an intrinsic solar Zn/Fe ratio, but later works (Vladilo 2002b) considered a possible nucleosynthetic enhancement of this ratio. Recovering the intrinsic abundances of the ISM is a very important goal, but applying dust corrections is a complex task, and, therefore, to take into account the uncertainties in the dust correction process, it is better to consider a variety of dust correction models, guided by some sensible assumptions about the chemistry of dust production in the ISM, and considering a range of nucleosynthetic contributions to the Zn/Fe ratio.

Constraining the nature of the DLAs is crucial for understanding the passage of a gas rich universe to the present day universe, where the directly observable baryonic content of galaxies is concentrated in stars. The DLAs are the dominant reservoir of neutral baryons at every observable epoch and are identified as the progenitors of modern galaxies, due to the correspondence of the inferred baryonic mass density of DLAs at $z \sim 2$ and the mass density in stars today (Storrie-Lombardi & Wolfe 2000). Since DLAs are the most directly observable baryonic mass systems at high redshift, their properties are an important constraint for theories of galaxy formation. One of the most exciting aspects of the DLAs is the fact that they provide a means for detecting galactic systems in the early stages of evolution. If DLAs are associated to one particular class of objects — e.g. disks, spheroids, galactic halos — their study allow us to follow the evolution of this population.

Nevertheless, the nature of the DLAs remains an intriguing problem. Results from early DLA surveys (Wolfe et al. 1986, Lanzetta et al. 1991) suggested that these systems could be the progenitors of the present day spirals. This hypothesis is supported by the kinematics of metal absorption lines exhibiting leading edge asymmetry, which could

be explained by large rotating disks (Prochaska & Wolfe 1997, 1998). However, Ledoux et al. (1998) found that the correlation of the broadening of the absorption lines ΔV with the asymmetry of the lines, expected in the disk interpretation, holds only for $\Delta V < 150 \text{ km s}^{-1}$, while the kinematics of the high ΔV DLAs is consistent with random motions, suggesting the merging of sub-systems, as expected in CDM models. In fact, the predictions of CDM cosmologies are often incompatible with the large disk interpretation. In hierarchical CDM models (Kauffmann 1996), high redshift galaxies should be relatively compact and underluminous in stark contrast with the presence of massive disks at $z \sim 3$. The semi-analytical models of Mo, Mao & White (1998), in which the DLAs are identified to centrifugally supported disks at the centre of dark matter halos, predict that most DLAs should be low surface brightness disks, with a median $V_{rot} < 100 \text{ km s}^{-1}$, pointing to low surface brightness galaxies (LSBs) rather than large disks as the main candidates for DLAs. On the other hand, the DLA data can be used to constrain semi-analytical models of galaxy formation, which include a variety of physical processes (Kauffmann & Haehnelt 2000, Somerville, Primack & Faber 2000). In addition, the CDM models have shown that the rotating disk interpretation for DLAs is not unique and that the kinematical data can also be reproduced by infalling sub-galactic clumps in collapsing dark matter halos (Haehnelt, Steinmetz & Rauch (1998). All these studies are consistent with a multi-population or multi-component scenario for the nature of DLAs. A multi-component scenario is suggested by the kinematics of the lines of high ions (CIV and SiIV), which indicate that the high ion subsystem is kinematically distinct from the low ion subsystem, although both subsystems are interrelated, as would be the case of a disk at the centre of a dark matter halo, filled with ionized gas radially infalling toward the disk (Wolfe & Prochaska 2000a,b).

The multi-population scenario, in which DLAs trace different types of galaxies, and not a single galaxy class, receives support from imaging studies of low redshift ($z_{abs} \lesssim 1$) DLAs (Le Brun et al. 1997; Pettini et al. 2000a; Turnshek et al. 2001), which reveal a variety of morphologies for DLA host candidates: spirals, compact dwarfs, low surface brightness galaxies. The luminosities of these objects also span a wide range: from a $\sim 0.01L_B^*$ LSB (Bowen et al. 2001) to a $3L_B^*$ spiral (Le Brun et al. 1997). At higher redshift, the data on DLA hosts are scarce. The three hosts of DLA at $z \gtrsim 2$ studied by Møller et al. (2002) are typically sub- L^* objects, and one of them has an irregular morphology.

The disagreement between some chemical evolution studies of DLAs is also suggestive of a multi-population scenario for DLAs. The controversy about the enhancement of the α elements in DLAs illustrates this point. Some studies (Pettini et al. 1997) found that the observed abundance pattern resembles those of the Galactic thin and thick disk, giving support to the disk scenario for DLAs. On the other hand, other authors (Molaro et al. 2001, Centurión et al. 2000) claimed that chemical enrichment of DLAs is characterized by an episodic or quiescent star formation regime similar to predictions of dwarf galaxy models (Matteucci et al. 1997).

In order to understand the nature of the DLAs, there have been several works comparing observations of DLAs

with the predictions of chemical evolution models. Matteucci et al. (1997) studied the α/Fe and N/O ratios observed in DLAs by means of chemical evolution models for starburst galaxies and the solar neighbourhood, and concluded that the most promising models to explain the observed abundances are those successfully describing dwarf irregular galaxies, which assume short but intense bursts of star formation. Jimenez et al. (1999) coupled a disk formation model to a chemical evolution model to investigate low surface brightness galaxies and high surface brightness galaxies, and conclude that LSBs could dominate the high z DLA population. Prantzos & Boissier (2000) and Hou, Boissier & Prantzos (2001) used chemical evolution models for disk evolution and showed how observational constraints on the metal column density of DLAs lead naturally to the observed mild redshift evolution of the abundances of several elements. Cen et al. (2002) used cosmological hydrodynamic simulations to compute the metallicity evolution of DLAs. In their models, the observed slow evolution of the DLA metallicity is explained by the steady conversion of the highest metallicities sites to galaxies, thus depleting this class, while all the lower metallicity systems show, individually, an increase in metallicity. Calura, Matteucci & Vladilo (2002) compared the observed chemical abundances to predictions of one-zone or multi-zone models of chemical evolution, and found that DLAs can be explained either by disks of spirals observed at large galactocentric distances, or by LMC-like irregular galaxies, or by starburst dwarf irregulars observed at different times after the last burst of star formation. Finally, we should mention the SPH simulations of Nagamine, Springel & Hernquist (2003), based on a conservative entropy formulation, and which include feedback by supernovae and galactic winds. The results of these simulations agree well with observations at $z = 3$ of the DLA abundance, their total neutral mass density, and column density distribution.

In the present work we compare the observations of DLAs with the predictions of three classes of models: i) one-zone models for dwarf galaxies; ii) multi-zone models for disk galaxies; iii) chemodynamical models for spheroids. The comparison with the results of the chemodynamical model represents a novelty of the present work, since, differently from the pure chemical evolution models, the chemodynamical models allow to calculate the gas flow in a consistent way instead of being introduced ad hoc. The connection between gas flows and star formation provides a natural explanation for the variety of chemical properties of DLAs. In addition, in the dwarf galaxy scenario for DLAs, the bursts occurs naturally, and one does not need additional model parameters characterizing the burst. Finally, the chemodynamical model, within the scenario in which the DLAs are dwarf galaxies, provides the properties of the DLA as a function of the galaxy impact parameter, which is not possible in the one-zone model. In this sense, the present work complements previous works, which, within the disk scenario for disks, study the properties of DLAs as a function of the galactocentric distance (Prantzos & Boissier 2001, Hou et al. 2001, Calura et al. 2003).

In section 2, we perform a statistical robust analysis of the available chemical abundance data for DLAs, and correct the abundances for dust depletion. Section 3 presents the classes of chemical evolution models used here. In sec-

tion 4, we apply models of distinct classes to examine several scenarios for DLAs. In Section 5, we summarise our results and, within the framework of the chemodynamical model of DLAs, we discuss the connection between gas flows and chemical evolution of galaxies, the epoch of galaxy formation, the evolution of the neutral gas content in DLAs, the metal content of the high-redshift Universe, and the relation between DLAs and LBGs. In this paper we adopt an $\Omega_m = 0.3$, $\Omega_\Lambda = 0.7$, $H_0 = 70 \text{ km s}^{-1} \text{ Mpc}^{-1}$ cosmology (the corresponding age of the universe is 13.47 Gyr).

2 ANALYSIS OF CHEMICAL ABUNDANCE DATA OF DLAS

In the past few years, the intense effort devoted to the spectroscopy of DLAs resulted in a large amount of chemical abundances derived for these systems. A compilation of chemical abundance measurements in DLAs based on the literature through early 2003 is shown in Table 1. All of the measurements in the table are from high (echelle) resolution obtained with 8-10 m telescopes. We consider abundance measurements of the following elements: N; Cr, Fe and Zn for the Fe-peak elements; O, Si and S for α -elements. Mg is not used as an α -element due to the difficulty in its determination and the uncertainties in its chemical evolution. Table 1 exhibits the HI density column $N(\text{HI})$ (cm^{-2}) in logarithm form, and the chemical abundances in the conventional notation $[X/H] = \log(X/H)_{\text{obs}} - \log(X/H)_\odot$. In this paper, the reference solar abundances $(X/H)_\odot$ are the N and O photospheric values of Holweger (2001), and the meteoritic values of Grevesse & Sauval (1998) for the other elements. Whenever the original paper listed in Table 1 uses a solar abundance set different from that above, the chemical abundances have been recomputed according to the solar abundances adopted here. We restrict the HI column densities to $\log N(\text{HI}) \geq 20.0$, in order for ionization corrections to be unimportant. Our DLA lower $\log N(\text{HI})$ cut-off is somewhat below the classical (Wolfe et al. 1986) limit of $\log N(\text{HI}) = 20.3$. The present work is concerned with the $[\alpha/N]$ and $[N/\alpha]$ ratios as diagnostic tools of chemical evolution of the DLAs. Therefore, Table 1 includes only DLAs with at least one chemical abundance measurement (actual determination or limit) of an α -element. Silicon is the most readily observed α -element, and the Si II 1808 Å transition is the most widely line used in the determination of the Si abundance in DLAs, since it is usually unsaturated allowing one to derive reliable Si II column densities. We then set $z = 0.85$ as the low redshift cut-off of our sample, because, at this redshift, the SiII λ 1808 line falls longward (at 3345 Å) of the atmospheric cut-off near 3200 Å.

2.1 Statistical Analysis

The data set of Table 1 is large enough to allow for the use of statistical methods in analysing abundances and abundance ratios in DLAs. Following the approach described by Ryan et al. (1996) we make use of robust statistical tools in order to define the best fit to the data, employing the techniques described by Cleveland & Kleiner (1975). Measurements for which only upper or lower limits are available are not included in the analysis. We obtain three resume

lines that summarise the trend of the data and are defined as follows: MM (midmean) - the average of all the points between and including the quartiles of the distribution over a given range, LSMM (lower semi-midmean) - the midmean for all the points below the median and USMM (upper semi-midmean) - the midmean for all the points above the median. If the data are scattered about the midmean according to a normal distribution, the semi-midmeans are estimates of the true quartiles of the distribution. In order to obtain the resume lines, two procedures, LOWESS and MSTAT, are applied to the data. LOWESS is an interactive procedure that smoothes a data distribution using a locally weighted robust regression according to the method described by Cleveland & Devlin (1988). This procedure reveals the trend of the distribution, while MSTAT analyses the spread along the correlation. In the LOWESS procedure, local regions around each data point are identified according to a smoothing parameter f ($0 < f < 1$), which controls the fraction of the data included in this region. Ideally one should try to choose a value of the smoothing parameter that is as large as possible without distorting patterns in the data. Suggested values are in the range 0.1 – 0.2; in this paper, we use $f = 0.1$. We refer the interested reader to the recent paper by Carretta et al. (2002), which computes summary lines similar to those used here, and which gives some additional references on the statistical methods and points to a code for the reader to use.

During the chemical evolution the elements of the Fe-peak group may follow a similar abundance pattern, as observed in the Milk Way metal-poor stars where chromium and zinc have abundance values close to iron. On the other hand, there is an overabundance of Zn compared to Cr and Fe in DLAs: in our sample $[\text{Zn}/\text{H}]_{\text{median}} = -1.04$ while $[\text{Fe}/\text{H}]_{\text{median}} = -1.58$ and $[\text{Cr}/\text{H}]_{\text{median}} = -1.36$ (Figure 1). This difference is generally attributed to the presence of dust in these systems (Pettini et al. 1994, 1997a), which would also affect the abundance of α elements, specially of silicon, which is highly depleted in the local ISM (Savage & Sembach 1996). Sulphur, on the contrary, is almost undepleted and could be used as a dust-free tracer of α elements in DLAs.

However, the $[\text{S}/\text{Si}]$ ratio in DLAs has a different behaviour from that expected in the local ISM: the median value of the systems that have absolute measurements of this ratio are close to solar ($[\text{S}/\text{Si}]_{\text{median}} = 0.01$). The statistical analysis exhibits the same trend: the median curve is on the solar value line, while the LSMM and USMM show little dispersion around $[\text{S}/\text{Si}] = 0$. This fact suggests that either the Si dust depletion is not significant in DLAs or that the S nucleosynthesis is a result of a contribution distinct from that in the local ISM. If both S and Si were perfect O tracers, the $[\text{S}/\text{Si}]$ ratio would have intrinsic solar values and the presence of dust (suggested in DLAs by the $[\text{Zn}/\text{Fe}]$ and $[\text{Zn}/\text{Cr}]$ ratios) would imply $[\text{S}/\text{Si}] > 0$. This is not the case, as one can see from Figure 2. DLAs exhibit both suprasolar and undersolar values of $[\text{S}/\text{Si}]$. Also stars of the Galactic thick disk show no sign of the α elements overabundance when S and Zn are used as tracers of α and Fe-peak elements: stars with $-1.2 < [\text{Fe}/\text{H}] < -0.4$ have an average $[\text{S}/\text{Zn}]$ of 0.03 ($-0.3 < [\text{S}/\text{Zn}] < 0.3$) (Prochaska et al. 2000). Matteucci & François (1989) have already interpreted the result of Diaz (1980) that the sulphur gradients

Table 1. Chemical Abundances in Damped Lyman α Systems.

QSO	z_{abs}	$\log N(\text{HI})$	[Zn/H]	[Cr/H]	[Fe/H]	[Si/H]	[S/H]	[O/H]	[N/H]	Ref. ^a
Q0000-2620	3.390	21.41±0.08	-2.07±0.10	-2.00±0.09	-2.04±0.09	-1.91±0.08	-1.91±0.09	-1.73±0.15	-2.61±0.12	6
QX00001	3.000	20.70±0.05	-	-	<-1.11	-1.81±0.05	-	-1.67±0.06	-3.22±0.06	10
Q0013-004	1.973	20.83±0.04	-0.75±0.06	-1.52±0.04	-1.51±0.05	-0.95±0.05	-0.74±0.04	-	-	18
BR0019-15	3.439	20.92±0.10	-	-	>-1.63	-1.06±0.10	-	-	-	8
Q0100+13 (PHL957)	2.309	21.40±0.05	-1.62±0.06	-1.69±0.05	-1.93±0.05	-1.37±0.05	-1.40±0.05	>-2.70	-1.96±0.35	8,4
Q0149+33	2.141	20.50±0.10	-1.67±0.10	-1.45±0.10	-1.77±0.10	-1.49±0.10	-	<0.56	-	8
Q0201+1120	3.386	21.26±0.08	-	-	-1.40±0.21	-	-1.25±0.18	-	-1.86±0.27	5
Q0201+36	2.463	20.38±0.04	-0.29±0.10	-0.80±0.05	-0.87±0.05	-0.41±0.05	-	-	>-1.31	8,10
Q0216+0803	1.769	20.00±0.18	<-0.33	<-0.63	-0.97±0.20	-0.67±0.21	-	-	-	2
Q0216+0803	2.293	20.45±0.16	<-0.31	<-0.75	-1.06±0.18	-0.56±0.16	-	-	-	2
J0255+00	3.253	20.70±0.10	-	-	-1.44±0.10	-0.94±0.11	-	-	-	8
J0255+00	3.915	21.30±0.05	-	-	-2.05±0.10	≥-2.67	-1.78±0.05	≥-2.87	-	8
Q0302-223	1.009	20.36±0.11	-0.58±0.12	-0.97±0.12	-1.19±0.12	-0.74±0.12	-	-	-	1
BR10307-4945	4.466	20.67±0.09	-	-	-1.97±0.19	-1.54±0.11	-	-1.50±0.19	-3.02±0.15	7
Q0336-01	3.062	21.20±0.10	-	-	-1.79±0.10	-	-1.41±0.10	>-1.00	>-2.09	8,10
Q0347-38	3.025	20.62±0.01	-1.50±0.05	-1.88±0.04	-1.69±0.01	-1.17±0.03	-	-0.73±0.06	-	3,10
Q0454+039	0.860	20.69±0.06	-1.03±0.12	-0.89±0.08	-1.02±0.08	-0.80±0.12	<-1.07	-	-	8
PKS0458-020	2.040	21.65±0.09	-1.19±0.09	-1.50±0.10	-1.77±0.10	>-1.17	-	-	-	8
PKS0528-2505	2.141	20.70±0.08	<-1.09	-1.29±0.09	-1.26±0.27	-1.00±0.09	-1.07±0.09	-	-2.05±0.11	2,19
PKS0528-2505	2.811	21.20±0.10	-0.78±0.12	-1.24±0.16	-1.25±0.15	-0.76±0.11	-	>2.00	≤-1.47	2,19
Q0551-366	1.962	20.50±0.08	-0.15±0.09	-0.92±0.10	-0.95±0.09	-0.44±0.10	-0.32±0.14	-	-	14
HS0741+4741	3.017	20.48±0.10	-	-	-1.93±0.10	-1.68±0.10	-	-	-2.44±0.10	8,10
Q0836+11	2.465	20.58±0.08	<-1.13	<-1.35	-1.40±0.10	-1.15±0.11	≤-1.12	-	-	8
Q0841+129	2.375	20.95±0.09	-1.51±0.10	-1.55±0.10	-1.58±0.10	-1.27±0.10	-1.38±0.09	-	-2.26±0.10	8,19
Q0841+129	2.476	20.78±0.10	-1.40±0.10	-1.61±0.10	-1.75±0.10	1.39±0.14	1.39±0.10	>-1.92	-2.59±0.10	8,19
Q0930+2858	3.235	20.18±0.10	-	-	≥-1.80	-	-1.71±0.15	>-2.38	-2.29±0.15	4
BRI0951-0450	3.857	20.60±0.10	-	-	-2.00±0.10	≥-1.53	-	-	-	8
BRI0951-0450	4.203	20.40±0.10	-	-	<-2.59	-2.62±0.10	-	-	-	8
PSS0957+33	4.178	20.50±0.10	-	-	-1.87±0.11	-1.50±0.10	-1.31±0.12	≥-1.90	-	8
PSS0957+33	3.279	20.32±0.08	≤-0.86	-	-1.45±0.08	-1.00±0.10	-	-	-	8
Q1055+4611	3.317	20.34±0.10	-	-	≥-1.61	≤-1.19	≥-1.97	≤-2.18	-	4
HE1104-1805	1.662	20.85±0.01	-1.04±0.01	-1.47±0.01	-1.58±0.02	-1.03±0.02	-	-0.79±0.20	-1.74±0.16	15
BRI1108-07	3.608	20.50±0.10	-	-	-2.12±0.10	-1.80±0.10	-	-	-	8
BRI1117-1329	3.350	20.84±0.13	-1.18±0.13	-1.36±0.13	-1.51±0.13	-1.26±0.13	-	-	-	13
BRI1202-0725	4.383	20.60±0.13	-	-	-2.22±0.16	-1.77±0.12	-	-	-	2,4
Q1210+17	1.892	20.60±0.10	-0.90±0.10	-1.00±0.10	-1.15±0.12	-0.87±0.10	-	-	-	8
GC1215+3322	1.999	20.95±0.07	-1.29±0.08	-1.52±0.10	-1.70±0.08	-1.48±0.07	-	>-2.56	-	8
Q1223+17	2.466	21.50±0.10	-1.62±0.10	-1.68±0.10	-1.84±0.10	-1.59±0.10	-	>-2.76	-2.60±0.18	8,10
Q1232+0815	2.338	20.80±0.10	-	-	-1.59±0.13	-1.18±0.13	-1.17±0.14	-	-2.10±0.13	19
MC1331+170	1.776	21.18±0.04	-1.30±0.05	-1.97±0.04	-2.06±0.05	-1.45±0.10	-	-	-1.82±0.10	8,10
BRI1346-0322	3.736	20.72±0.10	-	-	<-2.09	-2.33±0.10	-	≥-2.44	-	8
Q1351+318	1.149	20.23±0.10	-0.38±0.17	-0.94±0.17	-0.99±0.12	-0.56±0.17	-	-	-	16
Q1354+258	1.420	21.54±0.06	-1.63±0.16	-1.82±0.09	-2.02±0.08	-1.74±0.15	-	-	-	16
Q1409+095	2.456	20.54±0.04	-	-	-2.30±0.02	-2.01±0.02	-	-2.13±0.06	<-3.28	12
Q1425+6039	2.827	20.30±0.04	-	-	-1.33±0.04	>-1.03	-	-	-1.53±0.04	10
GB1759+7539	2.625	20.80±0.10	>-1.78	-1.26±0.10	-1.21±0.10	-0.82±0.10	-0.76±0.10	>-1.28	-1.53±0.02	8,10
Q1946+7658	2.843	20.27±0.06	-	-	-2.53±0.06	-2.23±0.06	<-1.98	-2.19±0.06	-3.61±0.07	8,10
Q2206-19	1.920	20.65±0.07	-0.41±0.07	-0.68±0.07	-0.86±0.07	-0.42±0.07	-	-	-	8
Q2206-199N	2.076	20.43±0.06	<-1.90	<-2.19	-2.61±0.06	-2.31±0.07	-	-1.94±0.09	<-3.49	8,12
Q2212-1626	3.662	20.20±0.08	-	-	≤-1.77	-1.91±0.08	-	≥-2.18	≤-2.55	2,4
LBQS2230+0322	1.864	20.85±0.08	-0.72±0.10	-1.12±0.10	-1.17±0.09	-0.75±0.10	-	-	-	8
Q2231-0015	2.066	20.56±0.10	-0.88±0.10	-1.06±0.10	-1.40±0.10	-0.87±0.10	-	-	-	8
Q2237-0608	4.080	20.52±0.11	-	-	-2.17±0.16	-1.81±0.11	-	-	≤-2.17	2,4
HE2243-6031	2.330	20.67±0.02	-1.12±0.05	-1.12±0.09	-1.25±0.02	-0.85±0.03	-0.85±0.03	-0.68±0.21	-1.72±0.02	11
B2314-409	1.874	20.10±0.20	<-1.21	<-1.62	-1.87±0.24	-1.87±0.22	<-1.66	≥-2.05±0.22	-	9
B2314-409	1.857	20.90±0.10	-1.04±0.14	-1.21±0.13	-1.32±0.14	-1.05±0.14	-1.00±0.18	-	-	9
Q2343+1230	2.431	20.35±0.05	-0.57±0.06	-	-1.19±0.06	-0.65±0.06	-0.83±0.08	>-1.73	-1.60±0.10	4,17
Q2344+124	2.538	20.36±0.10	-	-	-1.83±0.10	-1.74±0.10	<-1.36	>-2.07	-2.51±0.10	8,10
Q2348-01	2.615	21.30±0.10	≤-2.10	-2.30±0.12	-2.23±0.13	-1.97±0.12	-	-	-	8
Q2348-01	2.426	20.50±0.10	≤-1.46	-	-1.39±0.10	-0.69±0.10	-	-	-	8
Q2348-14	2.279	20.56±0.07	-	-	-2.24±0.10	-1.92±0.10	-2.03±0.10	-	<-3.26	8,10
Q2359-02	2.095	20.70±0.10	-0.77±0.10	-1.55±0.10	-1.65±0.10	-0.78±0.10	-	-	-	8
Q2359-02	2.154	20.30±0.10	<-1.07	-1.37±0.10	-1.88±0.10	-1.58±0.10	-	-	-	8

^aReferences: 1) Pettini et al. 2000a; 2) Lu et al. 1996; 3) Levshakov et al. 2002; 4) Lu et al. 1998b; 5) Ellison et al. 2001a; 6) Molaro et al. 2001; 7) Dessauges-Zavadsky et al. 2001; 8) Prochaska et al. 2001; 9) Ellison & Lopez 2001, 2002; 10) Prochaska et al. 2002b; 11) Lopez et al. 2002; 12) Pettini et al. 2002; 13) Péroux et al. 2002b; 14) Ledoux et al. 2002; 15) Lopez et al. 1999, 16) Pettini et al. 1999; 17) Dessauges-Zavadsky et al. 2002; 18) Petitjean et al. 2002; 19) Centurión et al. 2003.

are flatter than the oxygen ones in spiral disks as being due to differences between the production of O in SNe II, which grows with the progenitor mass from 10 M_{\odot} to 50 M_{\odot} , and that of S, which also occurs in high mass stars, but in a more restricted mass range though. This interpretation is consistent with chemical evolution models (Timmes et al. 1998) using the Woosley & Weaver (1995) yields for SNeII, that exhibit [S/Fe] strongly decreasing with [Fe/H] for [Fe/H] <-2. A third explanation (Izotov & Thuan 1999; Izotov, Schraerer & Charbonnel 2001) for the variations of S/Si is that ionization corrections for these elements are important, since S and Si are singly ionized and could also occur in HII regions (Viegas & Gruenwald 1991); in contrast, O is mostly neutral in H I gas. All these caveats should be kept in mind when using S as a proxy of α elements. Note, however, that the [O/Si] ratio in the sample has suprasolar values, $[O/Si]_{\text{median}} = 0.18$, which is well explained by the

dust depletion scenario, since O is essentially undepleted in the ISM. Unfortunately, in most cases the abundance of O is very uncertain because it is estimated from saturated lines; in this case, we use S as a proxy of O.

2.2 Dust Correction

The Si and Fe abundances are particularly important in the study of the $[\alpha/\text{Fe}]$ pattern, since Si and Fe are the elements tracing the α and iron peak group elements, respectively, with the largest number of abundance measurements for DLAs. However, since Fe and Si are refractory elements, they are expected to be depleted into grains. Ideally, one would like to gauge the level of dust depletion, and to apply dust corrections to the observed abundances in order to recover the intrinsic ISM (dust and gas phases) abundances.

In DLA studies, the classical indicator of dust deple-

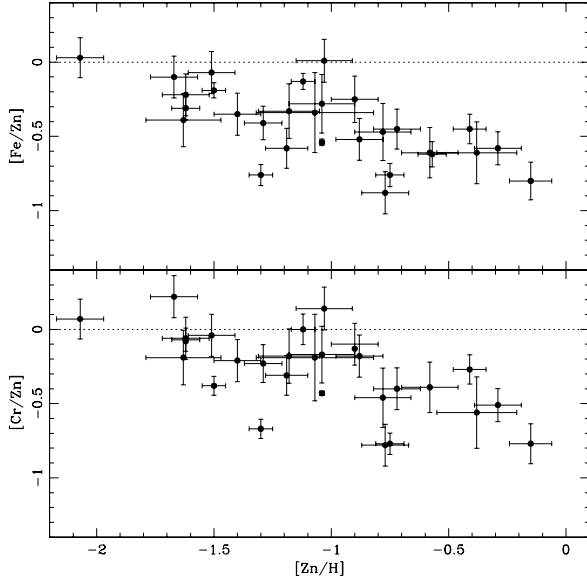


Figure 1. [Fe/Zn] and [Cr/Zn] vs. [Zn/H] observed in DLAs. The dotted line represents the solar value.

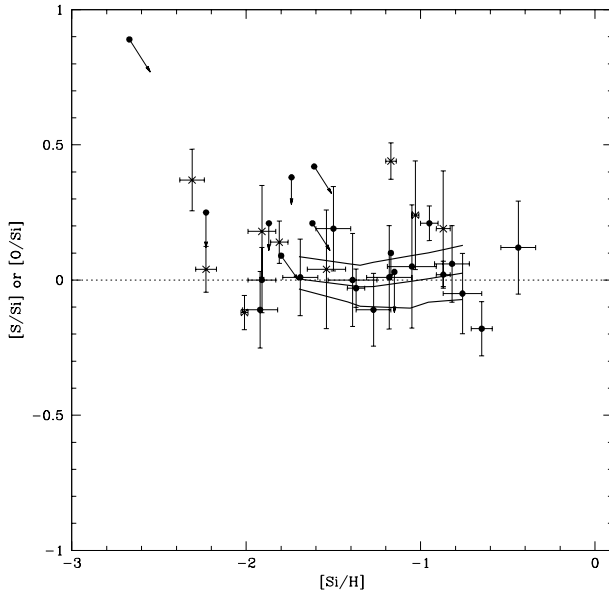


Figure 2. [S/Si] vs. [Si/H] (filled circles) and [O/Si] vs. [Si/H] (crosses) observed in DLAs. The dotted line represents the solar value. The heavy solid lines represent the robust statistical fits to [S/Si] vs. [Si/H]: MM (middle line), USMM (upper line) and LSMM (lower line).

tion has been the Zn/Fe (or Zn/Cr) ratio. Pettini et al. (1994) demonstrated that the majority of DLAs exhibit an enhancement of Zn relative to Cr. This overabundance have interpreted by them as an indication of dust depletion because Zn tends to track Fe in stars of all metallicity (Snedden, Gratton, & Crocker 1991), whereas Zn/Fe is enhanced in dust depleted regions of the ISM because Zn is mildly

refractory while Fe is heavily depleted (Savage & Sembach 1996, hereafter SS96)

However, recent stellar analyses have re-examined the Zn/Fe ratio in metal-poor and thick disk stars and have found enhanced Zn/Fe ratios (Johnson 1999, Prochaska et al. 2000, Umeda & Nomoto 2002). These surveys find an enhancement of $\approx +0.1$ in the Galactic thick disk stars ($[\text{Fe}/\text{H}] \approx -0.5$) (Prochaska et al. 2000) and a mean enhancement of $\approx +0.2$ to $+0.3$ in metal-poor stars ($[\text{Fe}/\text{H}] < -2$) (Johnson 1999). These results indicate the possibility of a nucleosynthetic contribution to the Zn/Fe enhancement of a given DLA. On the other hand, in the Galactic ISM, the suprasolar [Zn/Fe] and [Si/Fe] ratios provide evidence for dust depletion of Fe and Si, but the dust depletion pattern depends on the type of environment through which the sight line passes (SS96). SS96 consider four different dust depletion patterns corresponding to four types of Galactic ISM environment: (1) cool clouds in the Galactic disk (CD), (2) warm clouds in the disk (WD), (3) disk plus halo clouds (WHD), and (4) warm halo clouds (WH).

Applying dust corrections is a very complex issue, and, therefore, we considered a variety of dust correction models, based on the work of Vladilo (2002a). Following Vladilo (2002b), we apply the dust correction models of Vladilo (2002a) to our sample of DLAs with [Zn/Fe], [Fe/H] and [Si/H] measurements, in order to obtain the dust-corrected [Fe/H] and [Si/Fe] abundances. Our prescriptions, however differ from those of Vladilo (2002b) in that: i) we allow for a larger scatter in the nucleosynthetic contributions to the Zn/Fe enhancement by assuming a range for the intrinsic [Zn/Fe] ratio of $[\text{Zn}/\text{Fe}]_i = 0.0-0.2$, where Vladilo (2002b) considers $[\text{Zn}/\text{Fe}]_i = 0.0 - 0.1$; ii) we take as reference media the WD and the WH, whereas Vladilo (2002b) considers the WD and the CD. In fact, it is not appropriate to consider the cool clouds as a reference for the DLA environment, because the cool clouds exhibit levels of dust depletion ($[\text{Fe}/\text{Zn}]$, $[\text{Cr}/\text{Zn}]$, $[\text{Si}/\text{Zn}]$) much higher than those observed in DLAs, and the molecular hydrogen fractions are typically low in DLAs, in contrast to the large amount of molecules in the cool clouds. In addition, Savaglio, Panagia & Stiavelli (2000) have found, for 37 DLAs, that the majority ($\sim 60\%$) show a WH-like depletion pattern, then $\sim 30\%$ and $\sim 10\%$ have a WHD-like and WD-like depletion pattern, respectively. Finally, Hou et al. (2001) have found evidence for a dust depletion, for DLAs with large metal column density ($[\text{Zn}/\text{H}] + \log N(\text{H I}) > 19.8$), at a level (~ 0.4 dex) comparable to that observed in the WH clouds.

We summarize below the dust correction method of Vladilo (2002a). The dust correction method aims at obtaining the depletion of a given element X in the DLA:

$$\delta_X = [X/H]_{obs} - [X/H]_i \quad (1)$$

where $[X/H]_{obs}$ is the observed (gas) abundance and $[X/H]_i$ the intrinsic ISM abundance of the DLA. The depletion $\delta(X)$ is related to the fraction in dust of the element X, $f_X = N_{X,d}/N_{X,i}$, through:

$$f_X = 1 - 10^{\delta_X} \quad (2)$$

where $N_{X,d}$ is the column density of atoms X in the dust and $N_{X,i}$ the column density in the ISM (gas plus dust) of the DLA.

The fraction f_X is the relevant physical quantity, which

should scale with the amount of dust and with the abundance of X in dust. To derive this relation we express all abundances by number and relative to the abundance of a reference element Y (here we adopt iron as Y). Therefore, we define the relative abundance of X in the ISM as:

$$a_X = N_{X,i}/N_{Y,i}, \quad (3)$$

which is related to $[X/Y]_i$ through $a_X = 10^{[X/Y]_i}$. We also define the *reference dust fraction* (or *dust-to-metals ratio* as in Vladilo 2002a) in the ISM as f_Y .

We further assume that f_X depends on a_X and f_Y as:

$$f_X \propto f_Y^{(1+\eta_X)} a_X^{(\epsilon_X-1)}, \quad (4)$$

in which $(1+\eta_X)$ and (ϵ_X-1) are the power law indices of the power laws in f_Y and a_X , respectively. Eq. (4) allows us to obtain a general expression for f_X :

$$\frac{f_X}{f_{X,m}} = \left(\frac{f_Y}{f_{Y,m}} \right)^{(1+\eta_X)} \left(\frac{a_X}{a_{X,m}} \right)^{(\epsilon_X-1)}. \quad (5)$$

If $f_{X,m}$ is known for some reference medium m , and, if η_X and ϵ_X are known or assumed, we can obtain f_X . Here we use as reference environment m the warm disk (WD) of the Galaxy. Our values of $f_{X,m}$ correspond to $\delta_{X,m} = -0.43$, -1.095 , and -1.215 , for Si, Cr and Fe, respectively (Sembach & Savage 1996), and $\delta_{X,m} = -0.19$ for Zn (Roth & Blades 1995).

In Vladilo (1998), f_X was assumed to scale linearly with f_Y . However, this is correct when the dust composition does not vary with f_Y , a situation described by $\eta_X = 0$. However, studies of the Galactic ISM indicate that the dust composition changes with f_Y . In particular, for elements that are less depleted than the iron (e.g. silicon) the fraction in dust, in general, decreases faster than that of the iron for less depleted media, implying $\eta_X > 1$.

On the other hand, $\epsilon_X = 0$ implies that the dust composition is insensitive to variations of metallicity. However, one expects that the dust fraction would increase monotonically with the metallicity. In a simple physical picture, the two-body process of adhesion of an element onto dust grains should be proportional to the product of the densities of that element and the dust grains. If there are fewer atoms available, then the adhesion rate will be correspondingly lower. $\epsilon_X = 1$ follows from this picture, implying that the dust fraction scales linearly with the metallicity of the medium. Values of $\epsilon_X > 1$ could occur if three-body processes are important in the chemistry of dust production, but this is never the case in the low densities of the ISM. In addition, $\epsilon_X > 1$ not supported by studies of the ISM of the SMC (Vladilo 2002a). Therefore, the physically meaningful range for ϵ_X is $0 < \epsilon_X \leq 1$.

The value of η_X can be obtained from the comparison of knowledge of the dust depletion pattern in the local Galactic ISM, considering two different environments m and n . We assume that the abundances are constant in the solar neighbourhood. This implies that $a_{X,m} = a_{X,n}$ and, as a consequence, the scaling law, eq. 5, can be written in a simplified form:

$$\frac{f_{X,n}}{f_{X,m}} = \left(\frac{f_{Y,n}}{f_{Y,m}} \right)^{(1+\eta_X)}. \quad (6)$$

Here, the warm disk and the warm halo are the two

media used in the determination of η_X . For the warm halo, Sembach & Savage (1996) derive $\delta_{X,WH} = -0.26$, -0.51 , and -0.64 , for Si, Cr and Fe, respectively. In their study of Zn depletion in the Galactic ISM, Roth & Blades (1995) included one sightline of Sembach & Savage in the WH category, that toward HD167756, and, in addition, the WDH class sightline toward HD149881. They find for the sightlines toward HD167756 and HD149881, $\delta_{Zn,WH} = -0.05$ and -0.11 , respectively. Accordingly, in this work we assume $\delta_{Zn,WH} = -0.10$. However, assuming $\delta_{Zn,WH} = -0.05$ has little effect on our results (see Table 2). The corresponding values of η_X are 0.685, 0.450 and 1.760, for Si, Cr and Zn, respectively ($=4.922$ for Zn if $\delta_{Zn,WH} = -0.05$).

Once we have determined or estimated ϵ_X and η_X , we can proceed in our attempt of dust correction of the abundances, by considering the relation between the observed $[X/H]_{obs}$ and the intrinsic abundance $[X/H]_i$ (or $a_X = 10^{[X/Y]_i}$ in the equations below), which can be derived from Eq.s (1) and (5) above:

$$\left[\frac{X}{H} \right]_{obs} = \left[\frac{X}{H} \right]_i + \log \left\{ 1 - \rho^{(1+\eta_X)} a_X^{(\epsilon_X-1)} f_{X,m} \right\}, \quad (7)$$

where $\rho = f_Y/f_{Y,m}$ is the normalized (to $f_{Y,m}$ of the reference medium m) dust-to-metals ratio.

In order to recover the intrinsic abundances we first need to determine ρ . With this task, we apply Eq. (7) to the generic element X and to the reference element Y to obtain the relation:

$$\rho - \frac{f_{X,m} a_X^{\epsilon_X}}{f_{Y,m} 10^{[X/Y]_{obs}}} \rho^{(1+\eta_X)} + \frac{a_X - 10^{[X/Y]_{obs}}}{f_{Y,m} 10^{[X/Y]_{obs}}} = 0, \quad (8)$$

If we have a measurement of $[X/Y]_{obs}$ and a guess on $[X/Y]_i$, Eq. (8) can be solved to find the root ρ .

Once ρ is known, we can determine the intrinsic relative abundance $[X/Y]_i$ of a element X different from that used in Eq. (8) from the expression

$$a_X - \rho^{(1+\eta_X)} f_{X,i} a_X^{\epsilon_X} + (\rho f_{Y,m} - 1) 10^{[X/Y]_{obs}} = 0, \quad (9)$$

which is just a rearrangement of Eq. (8), with a_X as the unknown variable instead of ρ .

In applying the dust correction procedure of elemental abundances described above, we follow Vladilo (2002a), and consider eight dust models, based on our guesses on η_X and $[Zn/Fe]_i$. We consider $[Zn/Fe]_i$ as an input parameter to which we assign values 0.0 or +0.2 dex, in order to take into account a possible nucleosynthetic Zn/Fe enhancement. We adopt $\eta_X = 0$ or $\eta_X = 1$ as two limiting possibilities for η_X . As η_X is needed both for zinc in Eq. (8) in order to obtain ρ , and for the generic element X in Eq. (9), we consider that possibility that η_{Zn} and η_X are different. We have, therefore, eight possibilities: S00, S10, S01, S11, E00, E10, E01, and E11, where the letter S or E denotes solar $[Zn/Fe]_i = 0.0$ (S) or Zn enhanced $[Zn/Fe]_i = 0.2$ (E). The number code indicates the values of the pair $(\eta_{Zn}, \eta_X) = (0.0, 0.0)$ (00), $(1.0, 0.0)$ (10), $(0.0, 1.0)$ (01), and $(1.0, 1.0)$ (11). We should note that S00 and S10 (\equiv S0) and S01 and S11 (\equiv S1) are indistinguishable. In the case of iron abundances, S0 and S1 are indistinguishable, and also E00 and E10, and E01 and E11. For each dust correction model, the correction is applied to Si, Cr, Fe and Zn in the systems for which the observed $[Zn/Fe]$ is available.

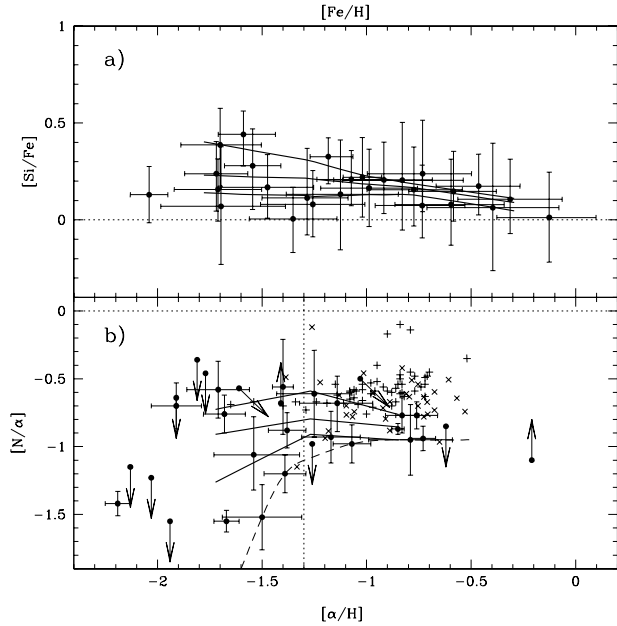


Figure 3. Upper panel: Dust-corrected $[\text{Si}/\text{Fe}]$ vs. $[\text{Fe}/\text{H}]$ for DLAs (filled circles). Also show $[\text{S}/\text{Fe}]$ vs. $[\text{Fe}/\text{H}]$ data (open circles). Lower Panel: $[\text{N}/\alpha]$ vs. $[\alpha/\text{H}]$ for DLAs and dwarf galaxies. The dwarf galaxy data are $[\text{N}/\text{O}]$ vs. $[\text{O}/\text{H}]$ from van Zee et al. (1997a,b) (crosses) and Izotov & Thuan (1999) (plus signs). For DLAs, we take as a proxy for α elements O or S, or, when not available, dust-corrected Si. The dotted horizontal lines represent the solar value, the dotted vertical line in the bottom panel the value $[\alpha/\text{H}] = -1.3$ (see text), and the heavy solid lines are the statistical fits to $[\text{Si}/\text{Fe}]$ vs. $[\text{Fe}/\text{H}]$ and $[\text{N}/\alpha]$ vs. $[\alpha/\text{H}]$ of DLAs. The bottom panel also shows the lower bound envelope to the $[\text{N}/\alpha]$ vs. $[\alpha/\text{H}]$ distribution of DLAs (dashed line).

Table 2 shows, for each system, the observed abundance ratios $[\text{Zn}/\text{Fe}]$ and $[\text{Si}/\text{Fe}]$ and the observed abundance of the iron $[\text{Fe}/\text{H}]$, the corrected abundances $[\text{Fe}/\text{H}]_{\text{cor}}$, the corrected abundance ratios $[\text{Si}/\text{Fe}]_{\text{cor}}$, for each dust correction model, and the averaged corrected $[\text{Fe}/\text{H}]_{\text{cor}}$ and $[\text{Si}/\text{Fe}]_{\text{cor}}$, $\langle [\text{Fe}/\text{H}] \rangle$ and $\langle [\text{Si}/\text{Fe}] \rangle$ (the average has been done over the eight possibilities S00, S01, S10, S11, E00, E01, E10 and E11). The error bars of $\langle [\text{Fe}/\text{H}] \rangle$ and $\langle [\text{Si}/\text{Fe}] \rangle$ encompass the range of average values predicted by each dust model and their respective 1σ errors. All models assume $[\text{Zn}/\text{H}]_{\text{WH}} = -0.1$ for the Galactic Warm Halo medium, but adopting $[\text{Zn}/\text{H}]_{\text{WH}} = -0.05$ changes very little our results even for the system with the largest $[\text{Zn}/\text{Fe}]_{\text{obs}}$, the $z_{\text{abs}} = 2.095$ DLA toward Q2359-02 (see Table 2).

2.2.1 The $[\text{Si}/\text{Fe}]$ ratio

The trend of the dust-corrected $[\text{Si}/\text{Fe}]$ ratio with metallicity ($[\text{Fe}/\text{H}]_{\text{cor}}$) is analysed with robust statistical methods (curves MM, USMM and LSMM in Figure 3a). In our sample, before any dust correction, the $[\text{Si}/\text{Fe}]$ ratio is typically suprasolar, with $[\text{Si}/\text{Fe}]_{\text{median}} = 0.32$. In the corrected sample, the $[\text{Si}/\text{Fe}]$ ratio is lowered to $[\text{Si}/\text{Fe}]_{\text{median}} = 0.16$, but remains suprasolar. Notice that the original dust correction procedure of Vladilo (1998) is equivalent to the case S0, which in general gives a larger downward correction for the

$[\text{Si}/\text{H}]$ ratio. After we perform a careful dust correction, we conclude that DLAs do exhibit $[\text{Si}/\text{Fe}]$ enhancement, and there is a trend of slight increase of $[\text{Si}/\text{H}]$ with decreasing metallicity, resembling that found for metal-poor stars of the Galaxy. This suggests that a number of DLAs may have had a chemical evolution similar to our Galaxy, supporting the scenario where these systems are the progenitors of disks. However, there are DLAs with nearly solar $[\text{Si}/\text{Fe}]$ ratio even at low metallicities, for which the disk picture does not apply. This case implies a slow star formation rate, which allows the SNe Ia to enrich the ISM with iron peak group elements. This behaviour is similar to that predicted by chemical evolution models for dwarf galaxies with bursts of star formation separated by quiescent periods (Matteucci et al. 1997), which allows that class of DLAs to be explained as (proto)dwarf galaxies. In summary, the $[\text{Si}/\text{Fe}]$ vs. $[\text{Fe}/\text{H}]$ distribution of DLAs does not exclude disks as DLA sites, but, if disks are present among DLA hosts, implies that they represent one component within a multi-population scenario.

2.2.2 The $[\text{N}/\alpha]$ ratio

The $[\text{N}/\alpha]$ ratio also allows one to constrain star formation times scales because of the delay of the injection of N with respect to α elements into the ISM. A nearly solar ratio ($[\text{N}/\alpha] = 0$) would indicate a slow star formation, during which there is enough time for production of N. Figure 3b show the trend $[\text{N}/\alpha]$ vs. $[\alpha/\text{H}]$ for DLAs and dwarf galaxies. The spread in the values of $[\text{N}/\alpha]$ observed in DLAs is larger than that observed in our Galaxy for stars in the same range of metallicity and in dwarf galaxies, and can be attributed to different formation epochs or chemical evolution histories for these systems. The high metallicity ($[\alpha/\text{H}] > -1.3$) DLAs exhibit values similar to those of dwarf galaxies giving support to the suggestion that DLAs could be the progenitors of dwarf galaxies. At lower metallicities, however, the $[\text{N}/\alpha]$ decreases, and there are DLAs with $[\text{N}/\alpha]$ values below that of any dwarf galaxy, which could be very young objects, for which there was no time for injection of N into the ISM.

Recently, Prochaska et al. (2002b) have claimed that the observed $[\text{N}/\alpha]$ ratios in DLAs present a bimodal distribution in the $[\text{N}/\alpha]$ vs. $[\alpha/\text{H}]$ plot, with a small sub-sample exhibiting significantly lower $[\text{N}/\alpha]$ ($[\text{N}/\alpha] \sim -1.5$) than the majority of systems. The authors consider that a way of naturally reproducing a bimodal distribution of $[\text{N}/\alpha]$ values is a top heavy IMF, thus reducing the nitrogen contribution of intermediate mass stars (IMS). The bimodality would severely challenge other explanations: the low $[\text{N}/\alpha]$ DLAs are observed during a transient period occurring within 250 Myr of a star burst and before the IMS have released their nitrogen into the ISM; N yields of IMS significantly decline with decreasing metallicity; the low $[\text{N}/\alpha]$ reflects the nucleosynthesis of Population III stars. Notice that a test of the top heavy IMF explanation would be that it predicts a high $[\alpha/\text{Fe}]$ ratio.

However, in our sample, the bimodality in the $[\text{N}/\alpha]$ vs. $[\alpha/\text{H}]$ plot is less apparent. Notice that we consider O, S, and Si_{cor} as the α -elements, while Prochaska et al. (2002b) use Si as a proxy of α -elements and do not consider dust-correction. In our sample, there are three systems with determinations of N and α abundances, which have low (~ -1.5) $[\text{N}/\alpha]$.

Table 2. Corrected abundance of Fe and Si.

QSO	z_{abs}	[Zn/Fe]	[Fe/H]	[Si/Fe]	[Fe/H] $_{cor}$	[Fe/H] $_{cor}$	Dust Model		[Si/Fe] $_{cor}$	[Si/Fe] $_{cor}$	[Si/Fe] $_{cor}$	⟨[Fe/H]⟩	⟨[Si/Fe]⟩
							S0	E00 E11					
Q0000-2620	3.390	-0.03±0.09	-2.04±0.09	0.13±0.07	-2.04±0.09	-2.04±0.09	0.13±0.14	0.13±0.13	0.13±0.13	0.13±0.13	-2.04 ^{+0.09} _{-0.09}	0.13 ^{+0.14} _{-0.14}	
Q0013-004	1.973	0.76±0.07	-1.51±0.05	0.56±0.06	-0.60±0.07	-0.89±0.07	0.00±0.04	0.12±0.07	0.10±0.06	0.10±0.06	-0.73 ^{+0.20} _{-0.22}	0.07 ^{+0.21} _{-0.17}	
Q0100+13	2.309	0.31±0.07	-1.93±0.07	0.56±0.06	-1.58±0.08	-1.82±0.07	0.28±0.10	0.46±0.11	0.46±0.12	0.47±0.10	-1.70 ^{+0.20} _{-0.19}	0.39 ^{+0.19} _{-0.21}	
Q0149+33	2.141	0.10±0.06	-1.77±0.10	0.28±0.06	-1.67±0.10	-1.77±0.10	0.19±0.15	0.28±0.12	0.28±0.12	0.28±0.12	-1.72 ^{+0.15} _{-0.15}	0.24 ^{+0.17} _{-0.19}	
Q0201+36	2.463	0.58±0.10	-0.87±0.05	0.46±0.06	-0.18±0.12	-0.46±0.10	0.03±0.07	0.15±0.10	0.14±0.10	0.14±0.10	-0.31 ^{+0.25} _{-0.25}	0.11 ^{+0.21} _{-0.18}	
Q0302-223	1.009	0.61±0.09	-1.19±0.12	0.45±0.09	-0.46±0.12	-0.74±0.12	0.01±0.08	0.13±0.11	0.11±0.11	0.11±0.11	-0.60 ^{+0.25} _{-0.27}	0.08 ^{+0.23} _{-0.21}	
Q0347-38	3.025	0.19±0.05	-1.69±0.01	0.52±0.03	-1.49±0.05	-1.69±0.02	0.34±0.07	0.52±0.04	0.52±0.04	0.52±0.04	-1.59 ^{+0.15} _{-0.12}	0.44 ^{+0.12} _{-0.16}	
Q0454+039	0.860	-0.01±0.13	-1.02±0.08	0.22±0.13	-1.02±0.09	-1.02±0.08	0.22±0.21	0.22±0.18	0.22±0.18	0.22±0.18	-1.02 ^{+0.09} _{-0.09}	0.22 ^{+0.21} _{-0.21}	
PKS0528-2505	2.811	0.47±0.14	-1.25±0.15	0.49±0.14	-0.70±0.16	-0.96±0.15	0.10±0.16	0.26±0.20	0.25±0.20	0.25±0.20	-0.83 ^{+0.29} _{-0.29}	0.20 ^{+0.30} _{-0.26}	
Q0551-366	1.962	0.80±0.08	-0.95±0.09	0.51±0.09	0.01±0.09	-0.29±0.09	-0.03±0.05	0.07±0.08	0.05±0.08	0.05±0.08	-0.13 ^{+0.22} _{-0.25}	0.01 ^{+0.23} _{-0.23}	
Q0841+129	2.375	0.07±0.08	-1.58±0.10	0.31±0.08	-1.51±0.10	-1.58±0.10	0.25±0.19	0.31±0.16	0.31±0.16	0.31±0.16	-1.54 ^{+0.14} _{-0.14}	0.28 ^{+0.19} _{-0.23}	
Q0841+129	2.476	0.35±0.06	-1.75±0.10	0.36±0.06	-1.35±0.10	-1.60±0.10	0.08±0.07	0.23±0.09	0.23±0.10	0.23±0.10	-1.47 ^{+0.22} _{-0.22}	0.17 ^{+0.17} _{-0.16}	
HE1104-1805	1.662	0.54±0.02	-1.58±0.02	0.55±0.03	-0.94±0.03	-1.22±0.02	0.10±0.03	0.26±0.04	0.24±0.04	0.24±0.04	-1.07 ^{+0.16} _{-0.16}	0.21 ^{+0.15} _{-0.14}	
BR1117-1329	3.350	0.33±0.07	-1.51±0.13	0.25±0.07	-1.14±0.13	-1.20±0.03	0.17±0.04	0.32±0.04	0.31±0.04	0.31±0.04	-1.26 ^{+0.25} _{-0.25}	0.08 ^{+0.17} _{-0.17}	
BR1210+17	1.892	0.25±0.09	-1.15±0.12	0.28±0.09	-0.88±0.12	-1.38±0.13	0.01±0.08	0.14±0.10	0.14±0.11	0.14±0.11	-1.26 ^{+0.25} _{-0.25}	0.08 ^{+0.17} _{-0.17}	
GC1215+3322	1.999	0.41±0.07	-1.70±0.08	0.22±0.06	-1.23±0.08	-1.38±0.13	0.02±0.10	0.15±0.10	0.15±0.11	0.15±0.11	-0.99 ^{+0.23} _{-0.23}	0.16 ^{+0.20} _{-0.20}	
Q1223+17	2.466	0.22±0.06	-1.84±0.10	0.25±0.06	-1.60±0.10	-1.48±0.08	-0.04±0.06	0.06±0.09	0.06±0.09	0.06±0.09	-1.35 ^{+0.21} _{-0.21}	0.00 ^{+0.16} _{-0.17}	
MC1331+170	1.776	0.76±0.06	-2.06±0.05	0.61±0.10	-1.15±0.06	-1.47±0.08	-0.07±0.10	0.07±0.10	0.07±0.10	0.07±0.10	-1.71 ^{+0.21} _{-0.21}	0.16 ^{+0.16} _{-0.16}	
Q1351+318	1.149	0.61±0.16	-0.99±0.12	0.43±0.16	-0.26±0.18	-1.82±0.10	0.09±0.09	0.23±0.08	0.23±0.08	0.23±0.08	-1.28 ^{+0.19} _{-0.22}	0.11 ^{+0.26} _{-0.19}	
Q1354+258	1.420	0.39±0.16	-2.02±0.08	0.28±0.15	-1.57±0.18	-1.39±0.06	0.06±0.13	0.24±0.13	0.22±0.13	0.22±0.13	-1.28 ^{+0.19} _{-0.22}	0.11 ^{+0.26} _{-0.19}	
Q2206-19	1.920	0.45±0.05	-0.86±0.07	0.44±0.05	-0.34±0.07	-0.54±0.17	0.00±0.13	0.11±0.19	0.10±0.19	0.10±0.19	-0.40 ^{+0.32} _{-0.32}	0.06 ^{+0.33} _{-0.33}	
LBQ2230+0322	1.864	0.45±0.09	-1.17±0.09	0.42±0.09	-0.65±0.10	-0.52±0.18	0.00±0.26	0.16±0.24	0.14±0.25	0.14±0.25	-1.70 ^{+0.31} _{-0.29}	0.07 ^{+0.31} _{-0.30}	
Q2231-0015	2.066	0.52±0.06	-1.40±0.10	0.53±0.06	-0.79±0.10	-1.82±0.16	0.01±0.15	0.13±0.21	0.12±0.22	0.12±0.22	-1.70 ^{+0.31} _{-0.29}	0.07 ^{+0.31} _{-0.30}	
Q2243-6031	2.330	0.13±0.05	-1.25±0.02	0.38±0.04	-1.12±0.05	-1.82±0.17	0.01±0.24	0.14±0.23	0.14±0.24	0.14±0.24	-0.46 ^{+0.20} _{-0.20}	0.17 ^{+0.16} _{-0.15}	
B2314-409	1.857	0.28±0.15	-1.32±0.14	0.27±0.15	-1.01±0.16	-0.60±0.07	0.08±0.06	0.23±0.07	0.22±0.08	0.22±0.08	-0.46 ^{+0.20} _{-0.20}	0.17 ^{+0.16} _{-0.15}	
Q2343+1230	2.431	0.62±0.06	-1.19±0.06	0.54±0.06	-0.45±0.07	-0.59±0.07	0.13±0.08	0.27±0.07	0.26±0.07	0.26±0.07	-0.77 ^{+0.23} _{-0.22}	0.16 ^{+0.22} _{-0.19}	
Q2359-02	2.095	0.88±0.06	-1.65±0.10	0.87±0.06	-0.60±0.10	-0.91±0.09	0.07±0.10	0.21±0.13	0.20±0.13	0.20±0.13	-0.92 ^{+0.23} _{-0.24}	0.21 ^{+0.20} _{-0.17}	
Q2359-02 ^a	2.095	0.88±0.06	-1.65±0.10	0.87±0.06	-0.62±0.10	-1.04±0.10	0.16±0.10	0.31±0.09	0.30±0.09	0.30±0.09	-1.18 ^{+0.12} _{-0.09}	0.33 ^{+0.10} _{-0.14}	
						-1.25±0.02	0.26±0.08	0.38±0.04	0.38±0.04	0.38±0.04	-1.12 ^{+0.28} _{-0.26}	0.13 ^{+0.28} _{-0.29}	
						-1.24±0.14	0.06±0.18	0.20±0.20	0.20±0.20	0.20±0.20	-1.12 ^{+0.28} _{-0.26}	0.13 ^{+0.28} _{-0.29}	
						-1.24±0.15	0.07±0.22	0.20±0.21	0.20±0.21	0.20±0.21	-1.12 ^{+0.28} _{-0.26}	0.13 ^{+0.28} _{-0.29}	
						-0.73±0.06	0.05±0.06	0.19±0.08	0.17±0.08	0.17±0.08	-0.58 ^{+0.20} _{-0.21}	0.15 ^{+0.21} _{-0.15}	
						-0.70±0.07	0.10±0.10	0.26±0.09	0.25±0.10	0.25±0.10	-0.58 ^{+0.20} _{-0.21}	0.15 ^{+0.21} _{-0.15}	
						-0.90±0.10	0.10±0.06	0.26±0.08	0.22±0.08	0.22±0.08	-0.73 ^{+0.23} _{-0.26}	0.24 ^{+0.28} _{-0.20}	
						-0.84±0.10	0.21±0.10	0.42±0.09	0.38±0.10	0.38±0.10	-0.73 ^{+0.23} _{-0.26}	0.24 ^{+0.28} _{-0.20}	
						-0.93±0.10	0.11±0.06	0.28±0.08	0.26±0.08	0.26±0.08	-0.77 ^{+0.24} _{-0.26}	0.26 ^{+0.27} _{-0.21}	
						-0.89±0.10	0.23±0.11	0.44±0.09	0.42±0.10	0.42±0.10	-0.77 ^{+0.24} _{-0.26}	0.26 ^{+0.27} _{-0.21}	

^a The dust models assume $[Zn/H]_{WH} = -0.05$ (see text).

Only one system, the DLA at $z = 2.843$ toward Q1946+7658 which happens to be that with the lowest metallicity in Figure 3, is isolated from the rest of the systems. The other two low $[N/\alpha]$ DLAs seem to be contiguous to the DLAs with higher $[N/\alpha]$.

Independently from a segregation of a low $[N/\alpha]$ subsample, to be confirmed by further observations, there seems to be a lower bound envelope in the $[N/\alpha]$ vs. $[\alpha/H]$ plot, extending in an arc from $([\alpha/H], [N/\alpha]) \sim (-1.5, -1.5)$ to $\sim (-0.7, -0.9)$. The two low $[N/\alpha]$ DLAs with $[\alpha/H] \sim -1.4$ are located along this envelope, forming a sequence with

higher $[N/\alpha]$ DLAs. This feature of the $[N/\alpha]$ vs. $[\alpha/H]$ distribution is interesting from the point of view of the models discussed in this work, since it corresponds to a maximum of the specific star formation rate ν (i.e. the inverse of the star formation time scale), which is a central ingredient of the chemical evolution process. Also the upper limits on $[N/\alpha]$ are consistent both with non-bimodality and an upper limit for ν .

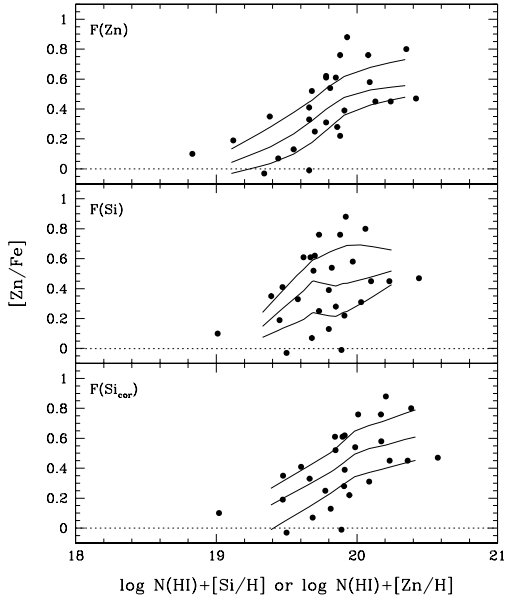


Figure 4. The trend of $[Zn/Fe]$ with the metal column density $F(X)$ for $X = Zn, Si,$ and Si_{cor} . The dotted line represents the solar value. The thick solid lines are the statistical fits to the DLA data.

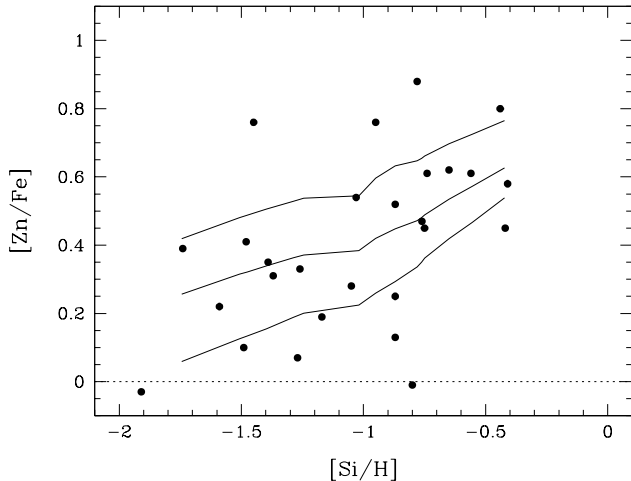


Figure 5. The trend of $[Zn/Fe]$ with $[Si/H]$ for the DLA sample with Zn, Fe and Si measurements. The dotted line represents the solar value. The thick solid lines are the statistical fits to the DLA data.

2.3 Estimating the dust depletion for DLAs without $[Zn/Fe]$ ratios

As any nucleosynthetic contribution to the $[Zn/Fe]$ ratio is small, not reasonably exceeding 0.3 dex, the $[Zn/Fe]$ enhancement is a reliable indicator of dust depletion. This is confirmed in Figure 4 from the good correlation between the observed $[Zn/Fe]$ ratio and the metal column density $F(Zn) = \log N(HI) + [Zn/H]$, which is used in the definition of “dust filter” by Prantzos & Boissier (2000), based on Boissé et al. (1998). The trend of increasing $[Zn/Fe]$ with $F(Zn)$

seems to flat beyond $F(Zn)$ somewhat below $F(Zn) = 20.0$. One could wonder if obscuration effects due the higher column density of metals would not prevent the highest depleted media from been seen. It is interesting to note that this apparent break in the trend occurs essentially at the same value of $F(Zn) = 19.8$, beyond which Hou et al. (2001) find evidence for dust depletion in DLAs.

If we consider the equivalent definition of $F(Zn)$ for the silicon, $F(Si) = \log N(HI) + [Si/H]$, the correlation is weaker. The reason for that, is that the weakly depleted zinc allows a much more reliable determination of the total metal column density than the Si, which is mildly depleted. However, if we use the dust corrected Si for the individual DLAs, we obtain a much more clear trend of $[Zn/Fe]$ with $F(Si_{cor})$. The correlation $[Zn/Fe] - F(Si_{cor})$ allow us to be more confident about the dust correction method used in this paper. In addition, the trend of increasing $[Zn/Fe]$ with $F(Si_{cor})$ flats for $F(Si_{cor}) \gtrsim 20$, which is the same behaviour exhibited by $F(Zn)$. However, in this case, the break seems to occur at a value of $F(Si_{cor})$ that is slightly higher that value of the break of $F(Zn)$. This would be expected if there is a modest enhancement of the $[Si/Fe]$ ratio.

The considerations above allow us to try to extend the sample of DLAs with estimated corrected abundances. In fact, only $\approx 40\%$ of the DLAs in our database have been selected to be applied the dust correction described in the last subsection, and important pieces of information could be missed. We would like to estimate intrinsic (dust-corrected) $[Fe/Si]$ ratios for systems without Zn measurements. In the following, we will try to use silicon as an indicator of dust depletion, or, equivalently, of the Zn/Fe ratio. Although silicon is a refractory element, its depletion is mild in lightly depleted regions of the ISM, and we have found that the corrections to be applied to Si were never large. The effects of dust depletion may hide significant trends with metallicity, and these effects can be reduced if we use a little refractory metallicity indicator. In fact, dust depletion has spoiled the correlation between $[Zn/Fe]$ and $F(Si)$, as we have already seen from the less clear trend of $[Zn/Fe]$ with $F(Si)$, when we use the observed (and therefore affected by dust) $[Si/H]$ instead of the dust-corrected $[Si/H]$. However, as we can see from Figure 5, there is a clear correlation between $[Zn/Fe]$ and $[Si/H]$, even using the observed $[Si/H]$.

As the $[Si/H]$ metallicity has been revealed to be a good predictor of the $[Zn/Fe]$ ratio, we will extend our sample of DLA with estimated dust depletion to include those DLAs which have a value of $F(Zn)$ too small for the Zn lines to be detected. Hereafter, this sample will be called the “no Zn sample”. It would allow us to explore a domain with smaller metallicities on average than the typical $[Fe/H] \gtrsim -2.0$ region defined by the original sample with Zn and Fe to which we applied the dust correction procedure.

The $[Zn/Fe]$ ratio, however, at least up to a metallicity $[Si/H] = -0.8$, varies between zero and values close to 0.8. Below $[Si/H] = -1.0$, the dispersion of $[Zn/Fe]$ becomes smaller and the largest values are bounded by the USMM of the statistical trends, with the exception of the $z_{abs} = 1.776$ DLA toward MC1331+170. This DLA, however, may be peculiar, since, in the sample used by Prochaska (2002) to investigate abundance variations within DLAs, it presents the second largest deviation from uniformity. In order to obtain the no Zn sample, we assume, for the systems with

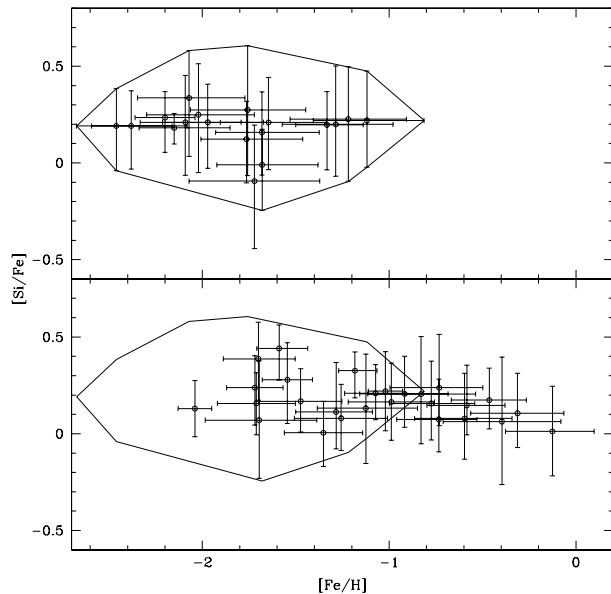


Figure 6. Upper panel: The $[\text{Si}/\text{Fe}]$ vs. $[\text{Fe}/\text{H}]$ distribution for the no Zn sample. Lower panel: Comparison of the $[\text{Si}/\text{Fe}]$ vs. $[\text{Fe}/\text{H}]$ distributions of the no Zn sample (represented by polygon enclosing this sample) with the sample with Zn, Fe and Si measurements.

measurements of Fe and Si, but not of Zn, and satisfying $[\text{Si}/\text{H}] \leq -1.0$, that the $[\text{Zn}/\text{Fe}]$ ratio varies between the USMM and the LSMM of the statistical trends shown in Figure 5, and then apply the dust correction method described in Section 2.2. We also use some useful upper limits whenever they define a narrower range of $[\text{Zn}/\text{Fe}]$ than that delimited by the USMM and the LSMM. It is the case of the DLAs toward PKS0528-2505 at $z = 2.141$ ($[\text{Zn}/\text{Fe}] < 0.17$), toward Q0836+11 at $z = 2.465$ ($[\text{Zn}/\text{Fe}] < 0.27$), and toward Q2348-01 at $z = 2.615$ ($[\text{Zn}/\text{Fe}] < 0.13$). The resulting estimates of the dust corrected abundances are shown in Figure 6. In Figure 6, the polygon encloses the no Zn sample. In drawing the polygon, we have excluded the DLA at $z = 1.874$ toward B2314-409, which has an unusually low observed $[\text{Si}/\text{Fe}]$ ratio (Ellison & Lopez 2001, 2002). Due to the uncertainties in the dust correction method and the two-step nature of the process used in building this sample, assigning dust-corrected abundances has no sense for individual DLAs but only for the sample as a whole. The no Zn sample seems to be an extension toward low metallicities of the sample with measurements of Zn, Fe and Si. It is not possible to know if the trend of increasing $[\text{Si}/\text{Fe}]$ with decreasing $[\text{Fe}/\text{H}]$ continues at $[\text{Fe}/\text{H}] < 2$ or if $[\text{Si}/\text{Fe}]$ reaches a plateau. For this sample, $[\text{Si}/\text{Fe}]_{\text{median}} = 0.204$, an enhancement only ~ 0.05 dex higher than that of the sample with Zn, Fe and Si measurements.

3 THE CHEMICAL EVOLUTION MODELS

In order to study the evolution of the metal content in DLAs, we use two classes of models: one-zone chemical evolution models and chemodynamical models. The one-zone chem-

ical evolution models are used to test the disk or dwarf galaxy scenario for DLAs, whereas the chemodynamical model checks for the dwarf galaxy scenario.

For each model class, a star formation law is specified. The stars formed follow a Salpeter IMF between 0.1 and 100 M_{\odot} . Chemical evolution occurs as the stars formed out of the ISM evolve and eject gas back into the ISM. The stars are assumed to die either as supernovae (SNe) or as planetary nebulae, when instantaneous ejection of mass, metals and energy occurs. The evolution of the abundances of He, C, N, O, Mg, Si, S and Fe is calculated by solving the basic equations of chemical evolution (see Matteucci & Tornambè 1987). We do not assume instantaneous recycling approximation for the chemical enrichment, but instead we take into account the delays for gas restoring from the stars due to the main-sequence lifetimes. Instantaneous mixing with the ISM is assumed for the stellar ejecta. The models start with an entirely gaseous protogalaxy or infalling gas with primordial chemical abundances ($Y = 0.24$, $Z = 0$).

In this work, we use metallicity dependent yields for SNe II, SNe Ia, and IMS. For SNe II, we use the metallicity dependent yields of Woosley & Weaver (1995), which are given for stars of mass $M = 12, 13, 15, 18, 20, 22, 25, 30, 35$ and 40 M_{\odot} and metallicities $Z/Z_{\odot} = 0, 10^{-4}, 10^{-2}, 10^{-1}$ and 1. Yields of SNIa resulting from Chandrasekhar mass white dwarfs, are taken from Iwamoto et al. (1999): their models W7 (progenitor star of initial metallicity $Z=Z_{\odot}$) and W70 (initial metallicity $Z=0$). The yields for IMS (0.8 – 8 M_{\odot}), with initial $Z=0.001, 0.004, 0.008, 0.02$ and 0.4, are from van den Hoek & Groenewegen (1997) (their variable η_{AGB} case). For more details of the nucleosynthesis prescriptions, see Friaça & Terlevich (1998, hereafter FT98).

Our choice of the mass (or surface mass density) and physical size of the model galaxies was based on the scenario in which the amount of gas in DLAs constitute a reservoir for the formation of present day galaxies, in view of the coincidence of the amount of mass in DLAs and the baryonic stellar mass in galaxies today (Storrie-Lombardi & Wolfe 2000). Therefore, the column density of the models should be not far from the baryonic column density of the present day galaxies being modelled. At the same time, the H I column densities predicted by all the models satisfy both our DLA definition, $\log N(\text{HI}) \geq 20.0$, and the high column density cut-off $\log N(\text{HI}) \lesssim 22$, observed in DLAs, and explained by Schaye (2001) as due the conversion of atomic hydrogen to molecular hydrogen in clouds with higher total hydrogen ($\text{HI} + \text{H}_2$) column density. Therefore, in comparing the observations with the predictions of the models, we will consider not only the abundances and abundances ratios, but also the H I column densities.

3.1 The one-zone chemical evolution models

Two types of one-zone chemical evolution models are used to explore the two most popular hypothesis for the nature of DLAs: disks (Prochaska & Wolfe 1997), and dwarf galaxies (Centurión et al. 2000, Molaro et al. 2001). One-zone models with galactic winds are used for dwarf galaxies, and multi-zone chemical evolution models with infall are used to represent disks.

3.1.1 The dwarf galaxy model

The dwarf galaxy model is the classical model with galactic winds (Matteucci 1994), first proposed by Larson (1974). In this model a wind is established at a time t_w when the thermal energy of the gas becomes higher than the potential energy, $E_{th,SN} > E_{b,gas}$. The wind instantly sweeps out all the gas of the galaxy and the star formation ceases. Later, processes of stellar mass loss restore the ISM.

Most of the models represent a galaxy with initial gas mass $M_G = 10^9 M_\odot$, but there is also a model with $M_G = 10^7 M_\odot$. The galaxies are inside a dark halo with a mass 7.5 times M_G . The star formation rate (SFR) is proportional to the present mass of gas and characterised by the specific star formation rate ν (the inverse of the star formation time scale). The fact that these models are simple, parameterized only in terms of ν makes them useful for gauging the effect of the star formation rate in the chemical evolution of DLAs. We run models for several values of ν ranging from 0.1 to 19 Gyr⁻¹. $\nu = 19$ Gyr⁻¹ follows from assuming $M_G = 10^9 M_\odot$ in the relation $\nu = 8.6(M_G/10^{12} M_\odot)^{-0.115}$ used in Matteucci & Tornambé (1987) and later works. The values of $\nu \leq 3$ Gyr⁻¹ reflect the typically low SFR of DLAs, as inferred from observations.

Interesting limits on the SFR of DLAs are given by imaging observations of the $z_{abs} = 3.386$ DLA toward Q0201+1120 (Ellison et al. 2001a). There are only two faints sources near the quasar with photometric redshifts consistent with the redshift of the DLA, the LBGs G2 and oM6 separated from the QSO by 4 and 2.9 arcsec. Spectroscopy of oM6 ($\mathcal{R}=23.97$ mag) revealed a prominent Lyman α emission line at $z_{em} = 3.645$. Therefore, oM6 is not the DLA. Rather, it is associated to the QSO (the difference in redshift between the oM6 and Q0201+1120 is only +465 km s⁻¹). G2, the remaining candidate for DLA, is so faint ($\mathcal{R}=25.3$) that there is no spectroscopy available. However, assuming that G2 is at the redshift of the DLA, we can estimate its SFR from its \mathcal{R} magnitude, because, at $z \sim 3$, the \mathcal{R} filter samples the rest-frame far-UV spectrum produced by recently formed O and B stars. Assuming that G2 has a typical DLA metallicity of $[\text{Fe}/\text{H}] = -1.5$ and that is undergoing continuous star formation for 10⁸ yr, we obtain, following Friaça & Terlevich (1999), a SFR of 6.2 M_\odot yr⁻¹. This corresponds to a model with $M_G = 10^9 M_\odot$ and $\nu = 6$ Gyr⁻¹ (or $M_G = 2 \times 10^9 M_\odot$ and $\nu = 3$ Gyr⁻¹). However, if G2 is not the DLA, then the absorber must be fainter than $\mathcal{R} \approx 26.0$, and the corresponding SFR $\lesssim 3 M_\odot$ yr⁻¹, or $\nu < 3$ Gyr⁻¹ for $M_G = 10^9 M_\odot$.

3.1.2 The disk model

The disk model belongs to the class of the models for the Galaxy with one infall episode of pristine gas. Following Matteucci & François (1989), the SFR depends on the galactocentric radius r through the total mass surface density $\sigma(r, t)$ and the gas fraction $G(r, t)$ as:

$$\Psi(r, t) = \tilde{\nu} \left[\frac{\sigma(r, t)}{\bar{\sigma}(\tilde{r}, t)} \right]^{2x_{SF}} \left[\frac{\sigma(r, t_G)}{\sigma(r, t)} \right]^{x_{SF}} G(r, t)^{(x_{SF}+1)}. \quad (10)$$

The normalisation $\tilde{\nu}$ of the SFR law is set at the solar position ($\tilde{r} = 8$ kpc) and at a galaxy age $t_G = 13$ Gyr (corresponding to a galaxy formation epoch $z_{GF} = 10$). We

assume $\tilde{\nu} = 0.5$ Gyr⁻¹ and $x_{SF} = 1/2$ in the adopted SFR law, in which the specific star formation rate depends on a power of the gas density $\nu \propto \rho^{x_{SF}}$. The infall rate into the disk is assumed to decrease with time as e^{-t/τ_D} , with the infall time scale τ_D given by:

$$\begin{aligned} \tau_D(r) &= 1 + 7/6(r-2), \text{ for } 2 \leq r \leq 8 \text{ kpc} \\ \tau_D(r) &= 8 + 0.5(r-8), \text{ for } r > 8 \text{ kpc} \end{aligned}$$

In this way, $\tau_D = 8$ and 1 Gyr at the solar position and at $r = 2$ kpc, respectively (Chiappini, Matteucci & Gratton 1997), and $\tau_D = 13$ Gyr at $r = 18$ kpc. An exponential surface mass density profile is adopted for the disk, $\sigma \propto e^{-r/r_G}$, with $r_G = 2.6$ kpc (Boissier & Prantzos 2000), normalized to $\sigma(\tilde{r}, t_G) = 50 M_\odot \text{ pc}^{-2}$ (Chiappini et al. 1997). We do not consider any threshold for star formation, differently from, for instance, Chiappini et al. (1997), who adopt the threshold $\Sigma_{th} = 7 M_\odot \text{ pc}^{-2}$. Adopting a threshold would impact on the outer regions of the disk, where it would induce a starburst-like star formation regime (Calura et al. 2002).

The disk model, the column density of HI implied by the present day total surface mass density is $4.7 \times 10^{21} \text{ cm}^{-2}$ at the solar radius and $1.0 \times 10^{20} \text{ cm}^{-2}$ at $r = 18$ kpc, which is consistent with the range of N(HI) values in DLAs. During the evolution of the disk (not in the very early phases, i.e. $t < \tau_D(r)$, when there is still very little gas in the disk), the value of the column density will vary by a factor of few around the values above.

3.2 The chemodynamical model

We investigate the scenario in which the DLAs are dwarf galaxies with the chemodynamical model of FT98, in which a single massive dark halo hosts baryonic gas that will fall toward the centre of dark halo and will subsequently form stars. The code combines a multi-zone chemical evolution solver and a 1D hydrodynamical code. The system, assumed to be spherical, is subdivided in several spherical zones and the hydrodynamical evolution of its ISM is calculated. The equations of chemical evolution for each zone are then solved taking into account the gas flow, and the evolution of the chemical abundances is obtained. A total of ≈ 100 star generations are stored during 13 Gyr for chemical evolution calculations. We assume that at a given radius r and at the time t , the specific star formation rate $\tilde{\nu}(r, t)$ follows a power-law function of gas density (ρ): $\tilde{\nu}(r, t) = \nu(\rho/\rho_0)^{1/2}$, where ρ_0 is the initial average gas density inside the core radius of the dark halo (r_h), and ν is the normalization of the star formation law. We include inhibition of star formation for expanding gas ($\nabla \cdot u > 0$) or when the density is too low, and, therefore, the cooling is inefficient (i.e., for a cooling time $t_{cool} = (3/2)k_B T / \mu m_H \Lambda(T) \rho$ longer than the dynamical time $t_{dyn} = (3\pi/16 G \rho)^{1/2}$) by multiplying $\tilde{\nu}$ as defined above by the inhibition factors $(1 + t_{dyn} \max(0, \nabla \cdot u))^{-1}$ and $(1 + t_{cool}/t_{dyn})^{-1}$. A characteristic of these models is that several episodes of inflow and outflow occur simultaneously at different radii. The chemodynamical model for spheroids was used to investigate the relation between young elliptical galaxies and QSO activity (FT98), the absence of passively evolving elliptical galaxies in deep surveys (Jimenez et al. 1999), LBGs (Friaça & Terlevich 1999), Blue Core Spheroids (Friaça & Terlevich 2001), and the coupled spheroid and black hole formation (Archibald et al. 2002).

We have extended the model family used in previous

works (FT98, Friaça & Terlevich 1999, 2001) toward lower masses to study dwarf spheroidals. The model dwarf galaxy has an initial gas mass $M_G = 10^9 M_\odot$, and the normalization of the SFR was set $\nu = 3$ or 1 Gyr^{-1} , rather than 10 Gyr^{-1} as for luminous ellipticals (in order to reproduce the suprasolar $[\text{Mg}/\text{Fe}]$ ratio of giant ellipticals). The scaling laws used in FT98, which are valid for giant or intermediate ellipticals, were changed to forms more appropriated for dwarf galaxies, using as reference the “bright dwarf ellipticals” defined in Bender, Burstein & Faber (1993): 1) $r_h = 1 \text{ kpc}$ was kept as in the $10^{10} M_\odot$ model, since dwarf galaxies have a larger radius with respect to their masses than bright ellipticals; 2) $r_{\text{tidal}}/r_h = 14$ instead of 28, used for luminous/intermediate ellipticals; 3) the Faber-Jackson relation was redefined in order to fit the pair NGC205-NGC3605. In FT98, the stellar population of the model galaxy follows a Faber-Jackson relation, $\sigma_* = 200(L_B/L_B^*)^{1/4} \text{ km s}^{-1}$, with L_B related to M_G through $[M/L_B] = 10$, the mass-light ratio typical of an L^* galaxy, or, equivalently, $\sigma_* = 150.5(M/10^{11} M_\odot)^{1/4} \text{ km s}^{-1}$. Here, we take the dynamical masses and velocity dispersions determined by Bender et al. (1993) for NGC205 and NGC3605 to obtain $\sigma_* = 188.3(M/10^{11} M_\odot)^{0.363} \text{ km s}^{-1}$. The initial HI column density of the model is $N(\text{HI}) = 1.65 \times 10^{21} \text{ cm}^{-2}$ through the centre of the galaxy.

4 INVESTIGATION OF DLAS WITH CHEMICAL EVOLUTION MODELS

4.1 One-zone model for dwarf galaxies

The predictions for $[\text{N}/\alpha]$ of the classic wind model for dwarf galaxies are compared to the observed ratios both in DLAs and dwarf galaxies in Figure 7. The observed $[\text{N}/\alpha]$ in DLAs shows a larger dispersion than that found for Galactic stars in the same range of metallicity and for dwarf galaxies. The different values of $[\text{N}/\alpha]$ for a given $[\alpha/\text{H}]$ can be explained by the different time scales for production of N and α elements, as one can see in the sequence of models with star formation ranging from almost quiescent ($\nu = 0.1 \text{ Gyr}^{-1}$) to violent ($\nu = 19 \text{ Gyr}^{-1}$). Most dwarf galaxies seem to require a specific star formation ν between 0.3 and 3 Gyr^{-1} , while the typical ν for DLAs seems to be somewhat lower, with a significant number of DLAs with $\nu \approx 0.1 \text{ Gyr}^{-1}$. For both populations, $\nu \approx 3 \text{ Gyr}^{-1}$ seems to be an upper limit for the efficiency of the SFR.

In our models, when the galactic wind occurs, the metallicity of the system is too high for a DLA. The time of the onset of the is galactic wind is $t_w = 0.16, 1.47$ and 5.66 Gyr , for $\nu = 19, 3$ and 1 Gyr^{-1} . The models with $\nu = 0.3$ and 0.1 Gyr^{-1} do not develop galactic wind until $t = 13 \text{ Gyr}$. The effect of the galactic wind is illustrated by the model with $M_G = 10^7 M_\odot$. When the galactic wind occurs at 0.3 Gyr , the star formation stops, and, consequently, the O release by SNII; however, the IMS keep ejecting N to the ISM. This is the reason for the upturn of the $M_G = 10^7 M_\odot$ model evolutionary track at $[\alpha/\text{H}] \approx 0.1$, away from the $M_G = 10^9 M_\odot$ model path.

The predictions for $[\text{Si}/\text{Fe}]$ of dwarf galaxy models with different values of ν are compared to the observed values in Figure 8. Most systems have $[\text{Si}/\text{Fe}]$ ratios below the predictions of any model. The classic wind model fails in explaining

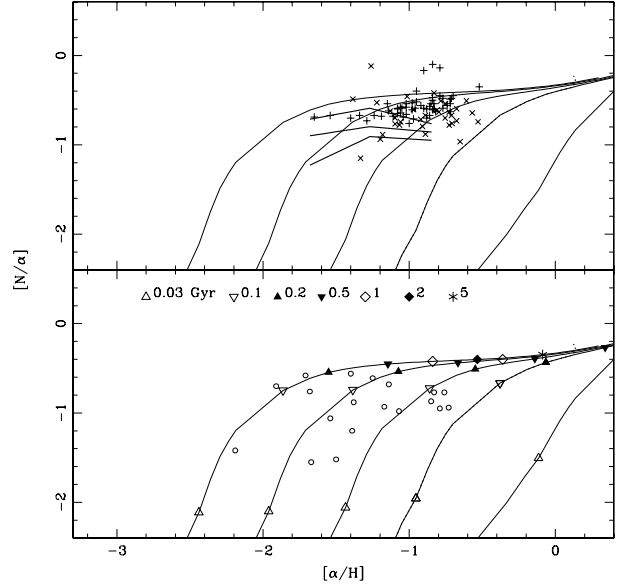


Figure 7. $[\text{N}/\alpha]$ vs. $[\alpha/\text{H}]$ observed in DLAs and dwarf galaxies compared with one-zone model predictions for dwarf galaxies. The solid lines represent the grid of models with $\nu = 0.1, 0.3, 1, 3, 19 \text{ Gyr}^{-1}$ (left to right), and the dotted line (barely seen) a model with $\nu = 3.0 \text{ Gyr}^{-1}$ and $M = 10^7 M_\odot$. Several evolutionary times are indicated by the symbols on the model lines. The lower panel exhibits the $[\text{N}/\alpha]$ vs. $[\alpha/\text{H}]$ data for DLAs (open circles), and upper panel the data for dwarf galaxies from van Zee et al. (1997a,b) (crosses) and Izotov & Thuan (1999) (plus signs). The α -element abundance is given by O for the model predictions and for the dwarf galaxy data, and for the DLA data, by O or S, or, when not available, by dust-corrected Si. The thick solid lines in the upper panel are the statistical fits to the DLA data.

a large number of systems with near-solar $[\text{Si}/\text{Fe}]$ ratios, unless we assume unrealistic, extremely low values of ν ($< 0.1 \text{ Gyr}^{-1}$).

4.2 One-zone model for disk galaxies

The disk models predictions are compared to the observed values in DLAs (Figures 9 and 10). There is a great dispersion for the $[\text{N}/\alpha]$ ratio, but the observed $[\text{N}/\alpha]$ ratios are confined to the region between $r = 4$ and 14 kpc , with a significant number of systems around $r = 8 \text{ kpc}$. The statistical trend lines seem to confirm the behaviour predicted by the models: the ratio increases with $[\alpha/\text{H}]$ rapidly in low metallicities and then becomes flatter. The plateau at higher metallicities is due to primary N production by IMS. The comparison between the observed $[\text{N}/\alpha]$ with the disk model predictions indicates star formation time scales in DLAs similar to those found in the solar neighbourhood. The lower bound envelope in the $[\text{N}/\alpha]$ vs. $[\alpha/\text{H}]$ distribution of the DLA data is nearly traced by the evolutionary track at $r = 4 \text{ kpc}$.

With respect to the $[\text{Si}/\text{Fe}]$ predictions from the disk model, the region $r \approx 8\text{--}18 \text{ kpc}$ accounts for most of the systems. There are, however, a few systems with higher $[\text{Si}/\text{Fe}]$ ratios implying a faster SFR than that found in outer regions of disks. The models also present the same increasing

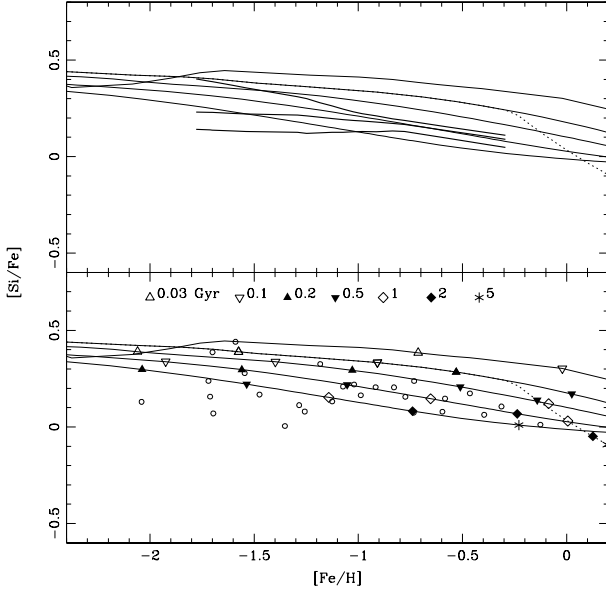


Figure 8. $[\text{Si}/\text{Fe}]$ vs. $[\text{Fe}/\text{H}]$ observed in DLAs (open circles) compared with one-zone models predictions for dwarf galaxies. The data points represent the dust-corrected abundances. The solid lines represent the grid of models with $\nu = 0.1, 0.3, 1, 3, 19 \text{ Gyr}^{-1}$ (bottom to top), and the dotted line a model with $\nu = 3.0 \text{ Gyr}^{-1}$ and $M = 10^7 M_{\odot}$. The thick solid lines in the upper panel are the statistical fits.

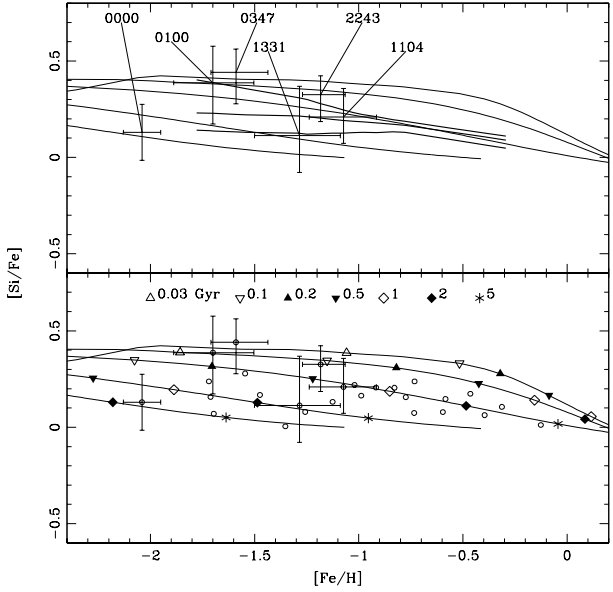


Figure 10. $[\text{Si}/\text{Fe}]$ vs. $[\text{Fe}/\text{H}]$ observed in DLAs (open circles) compared with chemical evolution models. The points represent the dust-corrected abundances. The solid lines are the predictions of the disk model at $r = 2, 4, 8, 14, 18 \text{ kpc}$ (top to bottom). The thick solid lines in the upper panel are the statistical fits. The points with error bars have the same meaning as in Figure 9.

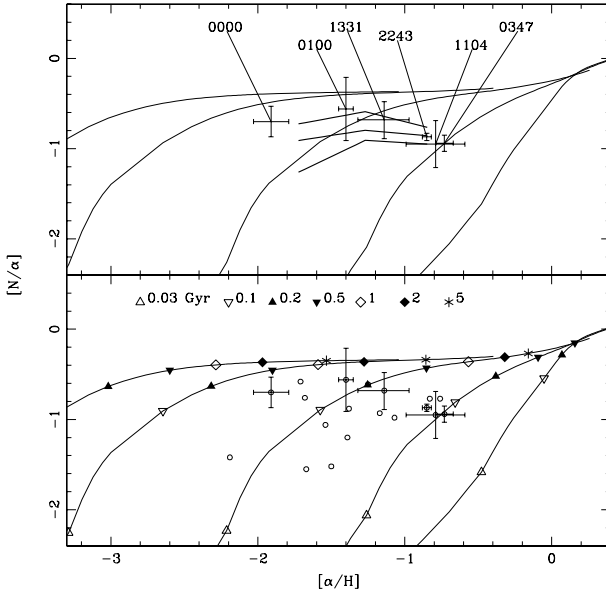


Figure 9. $[\text{N}/\alpha]$ vs. $[\alpha/\text{H}]$ observed in DLAs (open circles) compared with predictions from models of disk galaxies. The solid lines are the predictions of the disk model at $r = 2, 4, 8, 14, 18 \text{ kpc}$ (right to left). The thick solid lines in the upper panel are the statistical fits. The points with error bars refer to DLAs with both $[\text{N}/\alpha]$ and $[\text{Si}/\text{Fe}]_{\text{cor}}$ determinations, and are identified by the right ascension of the background QSO.

trend of $[\text{Si}/\text{Fe}]$ with decreasing $[\text{Fe}/\text{H}]$ of the data. Since external regions ($r \gtrsim 8 \text{ kpc}$) are favored as sites for DLAs, long star formation time scales are typical for these systems. A long and continuous star formation allows the iron peak group elements to be produced by SN Ia, giving rise to low values of $[\text{Si}/\text{Fe}]$. A slow star formation was also inferred from the analysis of the $[\text{N}/\alpha]$ ratios, but with the difference that more central regions ($r \approx 4 - 14 \text{ kpc}$) are required by the data. Although the $[\text{Si}/\text{Fe}]$ ratio apparently has a smaller dispersion than the $[\text{N}/\alpha]$ ratio, a number of systems have values of $[\text{Si}/\text{Fe}]$ too low or too high to be explained as arising in one characteristic portion of a disk. In addition, there are a few systems with $[\text{Si}/\text{Fe}]$ lower than that expected even in the outermost regions of a disk, and, for a number of DLAs, their low $[\text{Si}/\text{Fe}]$ and high $[\text{Fe}/\text{H}]$ could be achieved in the outer disk but at times later ($t \sim 5 \text{ Gyr}$ or later) than those allowed by the age of Universe at the DLA redshift.

Figure 11 presents the evolution the metallicity as a function of the H I column density predicted by the disk model for the radii $r = 2, 4, 8, 14, 18 \text{ kpc}$. This model for the Galactic disk predicts, at the outermost radius, metal column densities ($[\text{Si}/\text{H}] + \log N(\text{H I})$) that are too low at all times. The innermost radius that match the metallicity- $N(\text{H I})$ constraints is $r = 14 \text{ kpc}$, but only at late times, $t > 3 \text{ Gyr}$, thus limiting the applicability of this model to low redshift objects only. At the solar radius and $r = 4 \text{ kpc}$, the predictions match well the observations. The $r = 2 \text{ kpc}$ zone also satisfy the constraints in Figure 11, but only at very early times ($t \lesssim 5 \times 10^7 \text{ yr}$).

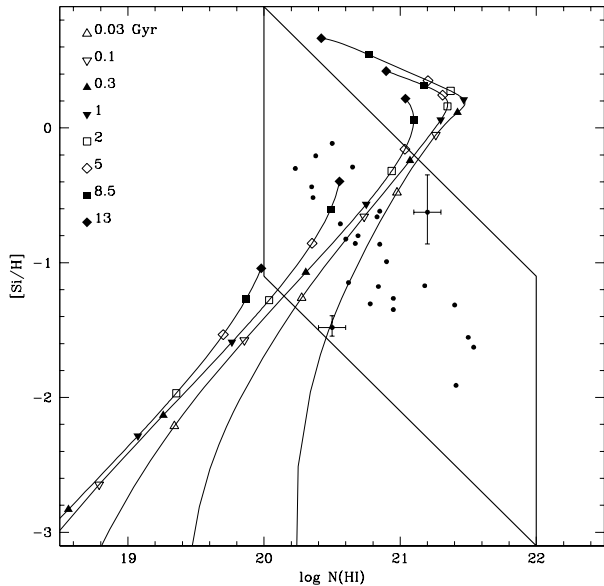


Figure 11. Metallicity vs. HI column density observed in DLAs compared with chemical evolution models. The metallicity is given by $[\text{Si}/\text{H}]_{\text{cor}}$ for the DLAs (filled circles). The solid lines are the predictions for disk models at $r = 2, 4, 8, 14, 18$ kpc (left to right). The thick line contour encloses the data according to the general constraints on HI column density for DLAs, $20 \leq \log N(\text{HI}) \leq 22$, and the limits on the metal column density of our sample, $F([\text{Si}/\text{H}]_{\text{cor}}) = [\text{Si}/\text{H}]_{\text{cor}} + \log N(\text{HI}) \leq 20.9$ (upper diagonal) and $F([\text{Si}/\text{H}]_{\text{cor}}) \geq 18.9$ (lower diagonal). For the sake of clarity, the errors are shown only for the two data points with the lowest and highest $F([\text{Si}/\text{H}]_{\text{cor}})$.

4.3 The chemodynamical model for dwarf spheroidal galaxies

The predictions for the $[\text{N}/\alpha]$ ratio of the chemodynamical model for dwarf spheroidal galaxies are compared to the observed ratios in Figures 12 and 13. One characteristic of the model is the occurrence of several short starbursts over the galaxy, which lead to rapid excursions of the evolutionary tracks in the $[\text{N}/\alpha]$ vs. $[\alpha/\text{H}]$ plane. Most of the systems are young, with ages around 0.1 Gyr or less (three systems, with $[\text{N}/\alpha] \sim -1.5$, have indicated ages of ~ 0.05 Gyr). The DLAs with $[\text{N}/\alpha] > -0.7$ and $[\alpha/\text{H}] < -1.0$ could be older systems ($t > 0.1$ Gyr), but the crowding of evolutionary tracks prevents us from assigning narrow ranges of ages (and of radii) to them.

The lower bound envelope in the $[\text{N}/\alpha]$ vs. $[\alpha/\text{H}]$ distribution of DLAs, which was reproduced by the one-zone dwarf galaxy model and by the disk model, representing an upper limit on ν , is even more apparent in the chemodynamical model with $\nu = 3 \text{ Gyr}^{-1}$, and corresponds to the radius $r \approx 1$ kpc.

The predicted and observed $[\text{Si}/\text{Fe}]$ ratios in DLAs are shown in Figures 14 and 15. Nearly all $[\text{Si}/\text{Fe}]$ values of DLAs are reproduced in the $r \sim 1 - 7$ kpc region, which is characterized by a low to intermediate star formation rate. As a consequence of the starbursts, at $r \sim 3$ kpc, the $[\text{Si}/\text{Fe}]$ ratio varies abruptly allowing the evolutionary track of the model to cover most of the data points. Multiple starburst

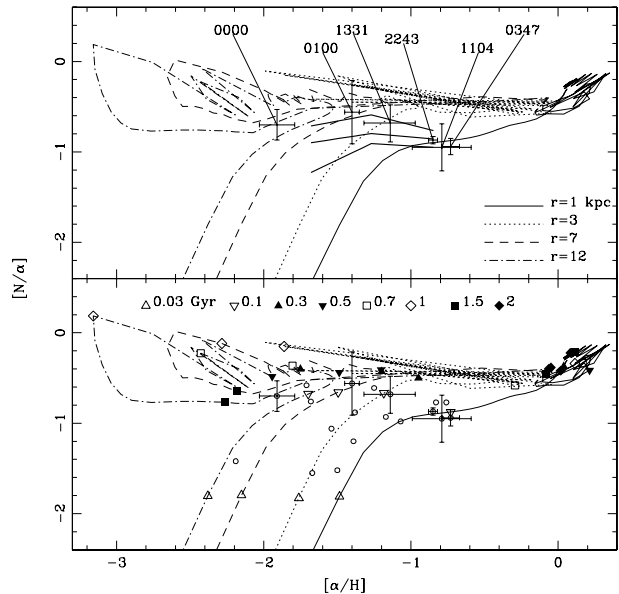


Figure 12. $[\text{N}/\alpha]$ vs. $[\alpha/\text{H}]$ observed in DLAs (open circles) compared to the predictions of chemodynamical model for dwarf spheroidal galaxies with $\nu = 3 \text{ Gyr}^{-1}$. The lines represent the model predictions at several radii. The thick solid lines in the upper panel are the statistical fits. The points with error bars have the same meaning as in Figure 9.

also happen at $r \sim 1$ kpc, although less dramatically seen in the $[\text{Si}/\text{Fe}]$ vs. $[\text{Fe}/\text{H}]$ diagram. The evolutionary tracks of the model show for $[\text{Fe}/\text{H}] < -2$ a trend of increasing $[\text{Si}/\text{Fe}]$ with decreasing metallicity which may be confirmed or not by the no Zn sample, with typically lower metallicities. More reliable abundance measurements in this range of metallicities are needed in order to establish whether there is discrepancy between the data and the models. Note that a potential discrepancy could be used as a test for the SNe II yields.

The occurrence of multiple starbursts and the peculiar tracks in both diagrams is explained by the connection between star formation and gas flows. In the dwarf galaxy model, there is a first infall episode of primordial gas into the dark matter halo potential well which ends with a starburst. This first starburst drives an outflow, which is very weak and it is reverted into infall by the large outer gas reservoir. During the outflow (except in its beginning) and the subsequent infall, the gas density is not high enough to allow star formation. Since the infall carries little enriched gas from the outer parts of the galaxy, there is a decrease in the metallicity of the gas as the infall goes on. Eventually the second infall builds up a gas density high enough to trigger a second starburst. In the inner regions of the galaxy, the cycle restarts a number of times giving rise to a series of bursts of star formation. In contrast, in the outer ($r \gtrsim 4$ kpc) regions of the galaxy, the cycle happens only once, and the gas succeeds in leaving the galaxy. Only this region presents a true galactic wind, which is enriched by SNe Ia. The plateau at low, constant $[\text{Si}/\text{Fe}]$ and $[\text{Fe}/\text{H}]$ increasing with time,

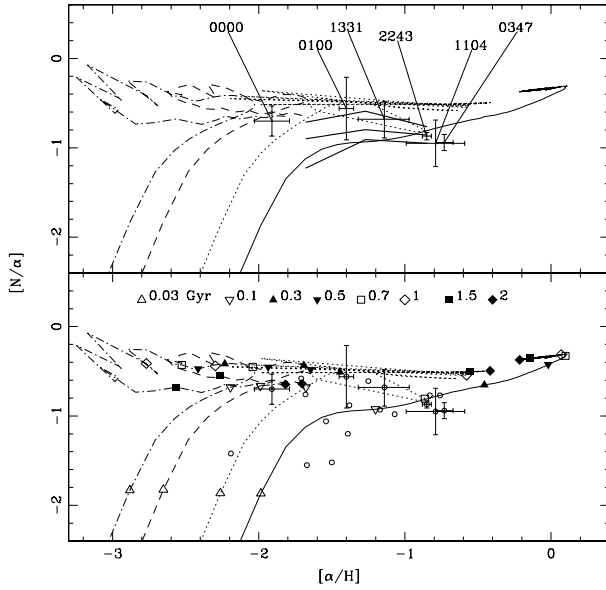


Figure 13. $[N/\alpha]$ vs. $[\alpha/H]$ observed in DLAs (open circles) compared to the predictions of chemodynamical model for dwarf spheroidal galaxies with $\nu = 1 \text{ Gyr}^{-1}$. The lines represent the model predictions at several radii. The meaning of the line styles is the same as in Figure 12. The thick solid lines in the upper panel are the statistical fits. The points with error bars have the same meaning as in Figure 9.

which is reached at $t \approx 1 \text{ Gyr}$ in the outer regions, marks the onset of the wind driven by SNe Ia. Therefore, dwarf spheroidal galaxies contribute to the enrichment of the intracluster medium mainly in iron and not in α elements (see Friaça 2000). The galactic wind is not a favourable site for DLAs — the low densities and high temperatures ($T \sim 10^7 \text{ K}$) make the cooling time too long for the development of thermal instabilities into DLAs — which accounts for the absence of DLAs in the galactic wind plateau.

Figure 16 shows the joint evolution of the H I column density and of the metallicity predicted by the chemodynamical model for several impact parameters. In this paper, we define as HI gas that with $T \leq 2 \times 10^4 \text{ K}$. During the evolution of the galaxy, part of the gas is heated mainly by SNe to temperatures higher than this limit. The hotter gas is not included in the calculation of the column density. At the start of the calculations the chemodynamical model exhibits $N(\text{HI}) = 1.23 \times 10^{21} \text{ cm}^{-2}$, through an impact parameter of 1 kpc (i.e. at $r = r_h$). The initial infall and, after a while, a series of starbursts are visible through excursions in the $\log N(\text{HI})$ vs. $[\text{Si}/\text{H}]$ diagram. The starbursts have a more dramatic effect in the $r = 3 \text{ kpc}$ region. In this region, the starbursts shift along the strip defined by the observational limits on the metal column density, toward higher metallicities and lower values of $N(\text{HI})$. In the outer regions ($r = 7$ and $r = 12 \text{ kpc}$), after the early infall, the galactic wind prevails and $N(\text{HI})$ is reduced dramatically. Note that at $r = 12 \text{ kpc}$, differently from at more central impact parameters, there is no initial increase of $N(\text{HI})$ due to the baryonic

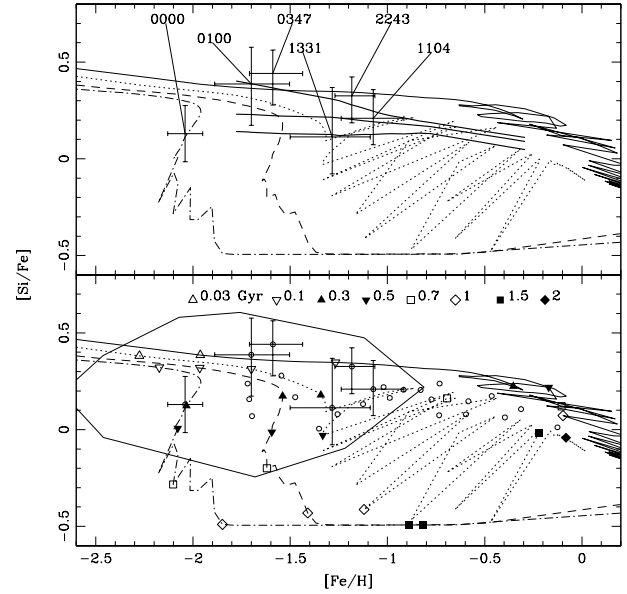


Figure 14. $[\text{Si}/\text{Fe}]$ vs. $[\text{Fe}/\text{H}]$ observed in DLAs (open circles) compared to the predictions of the chemodynamical model for dwarf spheroidal galaxies with $\nu = 3 \text{ Gyr}^{-3}$. The lines represent the model predictions at several radii. The meaning of the line styles is the same as in Figure 12. The thick solid lines in the upper panel are the statistical fits. The points with error bars have the same meaning as in Figure 9. The polygon encloses the no Zn sample defined in Section 2.3.

infall, and $N(\text{HI})$ remains below the lower limit for a DLA. Rather, the infall accumulates mass only in the inner regions of the galaxy. The outskirts of the galaxy ($r \gtrsim 10 \text{ kpc}$) would host only sub-DLAs and Lyman Limit Systems (LLSs). (sub-DLAs are QALs with $N(\text{HI}) = 10^{19} - 10^{20} \text{ cm}^{-2}$ — this range is narrower than that of the original definition of sub-DLAs, $N(\text{HI}) = 10^{19} - 2 \times 10^{20} \text{ cm}^{-2}$ [Péroux et al. 2002a], because we are considering as DLAs the QALs with $N(\text{HI}) > 10^{20} \text{ cm}^{-2}$; and LLSs are QALs with $N(\text{HI}) > 1.6 \times 10^{17} \text{ cm}^{-2}$ [Tytler 1982]) For a small impact parameter ($r = 1 \text{ kpc}$), the model satisfies the simultaneous constraints on $N(\text{HI})$ and metal column density of DLAs only during its early evolution ($t = 0.02 - 0.2 \text{ Gyr}$). At larger impact parameters, these constraints are satisfied during a long time span (from $t \sim 0.03$ to $> 1 \text{ Gyr}$). We did not try to tune the model to exactly match the observed values of $N(\text{HI})$. However, only a variation of a factor of two in the masses of the models accounts for the whole distribution of DLAs in the $\log N(\text{HI})$ –metallicity plane, as we see from Figure 16, where we show the results for a model with $\nu = 3 \text{ Gyr}^{-1}$ and $M_G = 5 \times 10^8 M_\odot$, and another with $\nu = 1 \text{ Gyr}^{-1}$ and $M_G = 5 \times 10^8 M_\odot$.

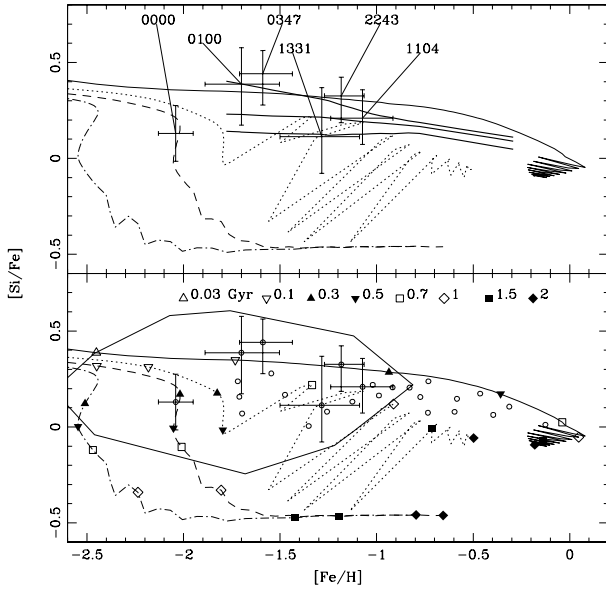


Figure 15. $[\text{Si}/\text{Fe}]$ vs. $[\text{Fe}/\text{H}]$ observed in DLAs (open circles) compared to the predictions of the chemodynamical model for dwarf spheroidals with $\nu = 1 \text{ Gyr}^{-3}$. The lines represent the model predictions at several radii. The meaning of the line styles is the same as in Figure 12. The thick solid lines in the upper panel are the statistical fits. The points with error bars have the same meaning as in Figure 9. The polygon encloses the no Zn sample defined in Section 2.3.

5 DISCUSSION

5.1 The abundance ratios

The presence of dust in DLAs is suggested by the undersolar $[\text{Cr}/\text{Zn}]$ and $[\text{Fe}/\text{Zn}]$ ratios (Pettini et al. 1994, 1999). This behaviour is generally attributed to the fact that Fe and Cr are refractory elements while Zn is little depleted, as seen in the ISM of the Galaxy. However, dust depletion is not so clearly indicated by the α elements: in most of the systems the $[\text{S}/\text{Si}]$ ratio is close to solar (but there are more DLAs with suprasolar $[\text{S}/\text{Si}]$ than with undersolar $[\text{S}/\text{Si}]$). The values above solar could be explained by taking into account the depletion pattern of the local ISM: while Si is depleted, S is nearly undepleted. On the other hand, the undersolar values, if real, are difficult to explain in these context. They may represent intrinsic values in DLAs, where the nucleosynthesis of S could result of contributions distinct from those of the local ISM, or could be explained in terms of differences in the ionization corrections for S and Si.

In DLAs, the $[\text{Si}/\text{Fe}]$ ratios, even after dust-correction, reveal the same α -element enhancement observed in metal-poor stars of the Galactic disk. However, there are systems with nearly solar $[\text{Si}/\text{Fe}]$ ratios, even at low metallicities, which is similar to the pattern predicted by dwarf galaxy models. This is consistent with a multi-population scenario for DLAs. However, the dwarf galaxy chemodynamical model accounts for nearly all the DLA data, while there are a number of systems not explained by the disk model.

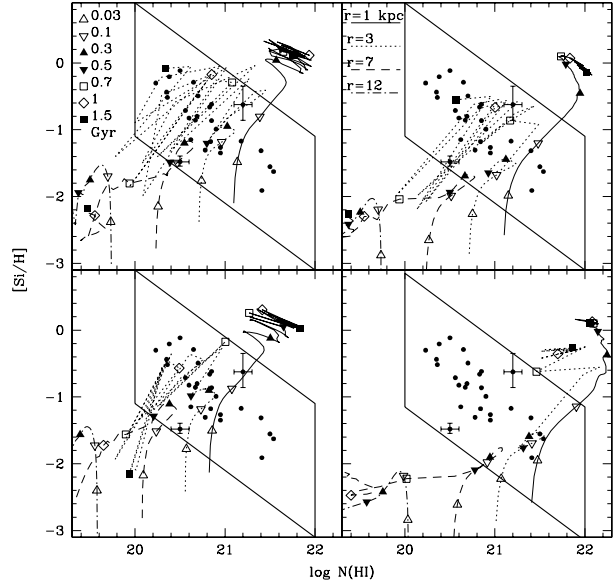


Figure 16. Metallicity vs. H I column density observed in DLAs compared to the predictions of the chemodynamical models for dwarf spheroidals with $M_G = 10^9 M_\odot$ and $\nu = 3 \text{ Gyr}^{-1}$ (upper left panel) and $\nu = 1 \text{ Gyr}^{-1}$ (upper right panel), with $M_G = 5 \times 10^8 M_\odot$ and $\nu = 3 \text{ Gyr}^{-1}$ (lower left panel) and with $M_G = 2 \times 10^9 M_\odot$ and $\nu = 1 \text{ Gyr}^{-1}$ (lower right panel). The lines represent the model predictions for several impact parameters. The meaning of the line styles is the same as in Figure 12. The metallicity is given by $[\text{Si}/\text{H}]_{\text{cor}}$ for the DLAs (filled circles). The thick line contour encloses the data according to the general constraints on HI column density for DLAs, $20 \leq \log N(\text{HI}) \leq 22$, and the limits on the metal column density of our sample, $F([\text{Si}/\text{H}]_{\text{cor}}) = [\text{Si}/\text{H}]_{\text{cor}} + \log N(\text{HI}) \leq 20.9$ (upper diagonal) and $F([\text{Si}/\text{H}]_{\text{cor}}) \geq 18.9$ (lower diagonal). For the sake of clarity, the errors are shown only for the two data points with the lowest and highest $F([\text{Si}/\text{H}]_{\text{cor}})$.

The pure chemical evolution models, both for disk systems and dwarf galaxies, present an apparent discrepancy (which is more serious for the dwarf galaxy models) between the fits to the $[\text{Si}/\text{Fe}]$ and $[\text{N}/\alpha]$ ratios. In the disk model, the $[\text{Si}/\text{Fe}]$ ratios are better reproduced at larger radii than those required by the $[\text{N}/\alpha]$ ratios, and, in the dwarf galaxy model, by lower values of ν than those implied by the $[\text{N}/\alpha]$ ratios. This difference could be related to an underestimated dust correction for Si, but it does not seem to be the case, since the trends $[\text{Si}/\text{Fe}]_{\text{cor}}$ vs. $[\text{Fe}/\text{H}]_{\text{cor}}$ and $[\text{S}/\text{Zn}]$ vs. $[\text{Zn}/\text{H}]$ are similar.

Another effect that could contribute to the above discrepancy is that different samples are used in the comparisons to the models. The DLA sample with $[\text{N}/\alpha]$ values is smaller than the sample with $[\text{Si}/\text{Fe}]_{\text{cor}}$ values. If a multi-population scenario for DLAs applies, some galaxy type missing or a few appearances of some rare galaxy type in the small number DLA sample with $[\text{N}/\alpha]$ values could make difficult the comparison between the two samples. In addition, the sample with $[\text{N}/\alpha]$ values has higher redshifts ($z_{\text{median}} = 3.02$) than the sample with $[\text{Si}/\text{Fe}]_{\text{cor}}$ values ($z_{\text{median}} = 2.07$), then one cannot exclude the possibility that the samples are drawn from different populations

(different galaxy types or galaxies at different evolutionary stages).

Differently from one-zone models, the chemodynamical model accounts for nearly all the DLA data. One single model (the $\nu = 3 \text{ Gyr}^{-1}$, $M = 10^9 M_\odot$ model) is able to reproduce $[\alpha/\text{Fe}]$ and $[\text{N}/\alpha]$ ratios and HI column densities of five out of six DLAs, if we consider a range of radii for the DLA sites — from central ($r \sim 1 \text{ kpc}$) to relatively outlying regions ($r \sim 7 \text{ kpc}$). Therefore, from the chemical point of view, the DLAs could represent a single type of system (the dwarf spheroids in our case). On the other hand, direct imaging (Le Brun et al. 1997; Pettini et al. 2000) and kinematical data (Prochaska et al. 1998) indicate that at least some DLAs are associated to disks. It is this sort of non-chemical evidence which makes a case for a multi-population scenario for DLAs.

We should note that for the system of our sample with the highest $[\text{Si}/\text{Fe}]$, the $z_{abs} = 3.025$ DLA toward Q0347-38, Levshakov et al. (2002) report $[\text{Si}/\text{Fe}] = 0.95 \pm 0.02$, which is significantly higher than the value $[\text{Si}/\text{Fe}] = 1.17 \pm 0.03$ of Prochaska et. (2002b) listed in Table 1. The reason for this difference is the lower $N(\text{Si}^+)$ measured by Prochaska et. (2002b), and not a higher $H(\text{HI})$, because Prochaska et. (2002b) adopt $\log H(\text{HI}) = 20.626 \pm 0.005$ from Levshakov et al. (2002). Prochaska et. (2002b) suggest that the discrepancy is due to significantly telluric line-blend in the spectrum obtained with the UVES-VLT by Prochaska et. (2002b). For this reason, we have adopted the $[\text{Si}/\text{H}]$ determination of Levshakov et al. (2002). However, if the high $[\text{Si}/\text{H}]$ is confirmed by further observations, it will pose problems both for the dwarf galaxy chemodynamical model and for the disk model, because the resulting $[\text{Si}/\text{Fe}] = 0.74$ will be much higher than the predictions of any model presented here. If this is the case, it may represent a system with a SFR higher (e.g. $\nu = 10 \text{ Gyr}^{-1}$) than that assumed in the dwarf galaxy chemodynamical model ($\nu = 3 \text{ Gyr}^{-1}$).

5.2 The role of gas flows in DLAs

The failure of the one-zone model for dwarf galaxies in reproducing the abundance ratio data is related to a general inability of the classic wind models, which lead Matteucci et al. (1997) to propose a multi-burst model for DLAs, based on a single-zone chemical evolution model for dwarf irregular, with a series of parameters describing the burst – burst duration, number of bursts, interval between bursts. In the chemodynamical model, multiple star bursts appear in a natural way, and no ad hoc parameters describing them are needed. The inner ($r \lesssim 4 \text{ kpc}$) region exhibits a series of short bursts of star formation, which can be seen very clearly in the $[\text{Si}/\text{Fe}]$ vs. $[\text{Fe}/\text{H}]$ plot, and which cover all the values derived for the DLAs. The connection between the gas flow evolution and the star formation rate is the reason behind the ability of the chemodynamical model in reproducing the wide range of abundance ratios seen in DLAs.

The success of the chemodynamical model for dwarf galaxies does not represent an argument against the disk scenario for DLAs, because we chose a simple model for the disk evolution, that with a single infall of primordial gas, in order to discern the effect of gas flows in the evolution of the system (for the same reason, we studied the classic galactic wind model for dwarf galaxies). The disk paradigm

for DLAs should be tested by more sophisticated models, such as the double infall model for the Galaxy (Chiappini et al. 1997). Moreover, the fact that this model considers a more elaborated form for infall stress the importance of gas flows in chemical evolution of galaxies. Kinematical data, revealing the velocity field underlying the DLAs would be very useful for checking distinct DLA scenarios. However, as a preliminary conclusion, our results seem to exclude an outflow scenario for DLAs, since our model resolves outflows, and no DLA is found in the outflow stage/region.

5.3 The epoch of galaxy formation

An important implication of the study of the chemical evolution of DLAs is to investigate the cosmic progress of galaxy formation. The models provide chemical clocks to infer the formation epoch of spheroids using the DLA chemical data as constraints. We will use as simultaneous constraints on the epoch of galaxy formation z_{GF} , the $[\text{N}/\alpha]$ vs. $[\alpha/\text{H}]$ and $[\text{Si}/\text{Fe}]$ vs. $[\text{Fe}/\text{H}]$ data of six DLAs, which are compared with the predictions of the chemodynamical models with $M_G = 10^9 M_\odot$ and $\nu = 3$ and 1 Gyr^{-1} . The systems can be divided in 2 groups according to the region of the galaxy reproducing the $[\text{N}/\alpha]$ ratio: the inner DLAs, located at $r \sim 1 \text{ kpc}$ (DLAs toward Q1104-1805, Q2243-6031 and Q0347-38), and the outer DLAs, in the $r \sim 3 - 7 \text{ kpc}$ region (DLAs toward Q0000-2620, Q0100+13 and Q1331+17). The model with $\nu = 3 \text{ Gyr}^{-1}$ best fit the inner DLA data. The system toward Q0000-2620 is fitted only by the $\nu = 1 \text{ Gyr}^{-1}$ model, but it probably has $M_G = 2 - 3 \times 10^9 M_\odot$, from the constraints on $N(\text{HI})$. We can see that the inner DLAs would be within very young galaxies, with ages $\sim 0.1 \text{ Gyr}$. Only far from the centre, we find older systems: the DLAs toward Q0000-2620, Q0100+13 and Q1331+17, with ages of 0.1-0.5, 0.1-0.3 and 0.5-1.0 Gyr, respectively, corresponding to $z_{GF} = 3.558-4.411$, $2.392-2.574$, and $2.075-2.465$. The galaxy formation epoch of a DLA in very young environment is, of course, only slightly higher than its z_{abs} . Assuming an age of 0.1 Gyr, the DLAs toward Q0347-38, Q1104-1805, and Q2243-6031 have been formed at $z_{GF} = 3.160$, 1.711 , and 2.414 , respectively. These numbers characterize a typical epoch of formation for these systems around $z_{GF} \sim 2 - 3.5$ within a range $z_{GF} = 1.7 - 4.5$. Higher values of z_{GF} could be achieved if we consider the systems with highest values of $[\text{Fe}/\text{H}]$, supposed to be the most chemically evolved, and good candidates to be old systems. This is the case of the DLAs toward Q0551-366 ($z_{abs} = 1.962$) and Q0201+36 ($z_{abs} = 2.463$), with $[\text{Fe}/\text{H}]_{cor} = -0.013$ and -0.191 respectively, which are in a region of the $[\text{Fe}/\text{H}]$ vs. $[\text{Si}/\text{Fe}]$ plane corresponding to galaxy ages of 1-2 Gyr. Very early galaxy formation could occur: $z_{GF} = 2.791-4.579$ and $3.794-8.147$, for Q0551-366 and Q0201+36, respectively. One general conclusion is that DLAs constitute a relatively young population with ages not exceeding 2 Gyr, or even 1 Gyr.

5.4 Neutral gas content of DLAs

While the directly observable baryonic content of galaxies at the present epoch is concentrated in stars, in the past, this must be in the form of gas. The near coincidence of the inferred baryonic mass density of DLAs (Ω_{DLA}) at $z \sim$

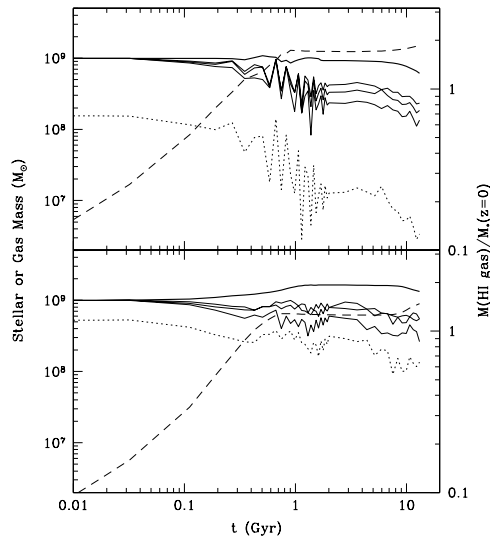


Figure 17. Evolution of the baryonic content of the models with $M_G = 10^9 M_\odot$, for $\nu = 3 \text{ Gyr}^{-1}$ (upper panel) and $\nu = 1 \text{ Gyr}^{-1}$ (lower panel). The thin solid lines give the evolution of the mass in neutral gas for three temperature limits ($T \leq 10^4$, 2×10^4 and $3 \times 10^4 \text{ K}$). The solid line is the evolution of the total amount of gas (at any temperature). The dashed line represents the evolution of the stellar mass. Also shown the evolution of the neutral gas fraction with respect to the stellar mass at $z = 0$, assuming that the galaxy has been formed at $z = 4.5$ (dotted line).

2 and the mass density in stars today (Storrie-Lombardi & Wolfe 2000) makes the DLAs the prime candidates to the progenitors of modern galaxies. Since the DLAs are the dominant reservoir of neutral (HI) gas at $z > 0$ available for galaxy formation, it is of interest to establish whether the dwarf galaxy chemodynamical model predicts enough HI gas to make the DLAs important contributors to the present day stellar mass of the universe. In addition, the evolution of the H I mass in our models should be compared to recent estimates of the evolution of Ω_{DLA} (Rao & Turnshek 2000; Storrie-Lombardi & Wolfe 2000; Péroux et al. 2001).

Figure 17 shows the evolution of the HI gas for the models with $M_G = 10^9 M_\odot$, and $\nu = 3 \text{ Gyr}^{-1}$ and $\nu = 1 \text{ Gyr}^{-1}$. We assume that the neutral gas contains only HI and no H_2 , since our calculations do not include molecules. Our adopted cooling function is valid down to $T = 1900 \text{ K}$, where the H_2 fraction is still unimportant. Any gas that cools below this temperature is removed from the fluid according to our prescriptions for thermal instabilities (Friaça 1993, Friaça & Jafelice 1999, Gonçalves & Friaça 1999), and is used in star formation. The identification of the HI gas to the neutral gas is supported by the fact that in DLAs $N(\text{H}_2) \ll N(\text{H I})$ (Petitjean, Srianand & Ledoux 2002). We consider as HI gas that with $T \leq 2 \times 10^4 \text{ K}$. This upper temperature limit is somewhat higher than the typical $\approx 10^4 \text{ K}$ of the warm medium in the Galactic disk, but in the halo warm medium, the temperatures may be considerably higher than in the disk warm medium (Sembach & Savage 1996). In addition, Prochaska et al. (2002a) derived from the Doppler parameters

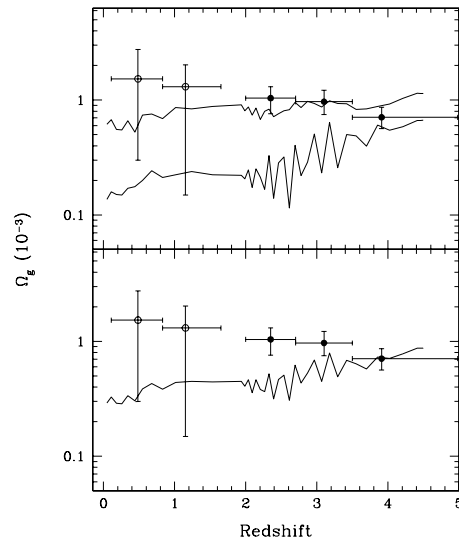


Figure 18. Comparison of the observed evolution of the Ω_g due to the DLAs to the predictions of the dwarf galaxy chemodynamical models with $M_G = 10^9 M_\odot$, assuming that the dwarf galaxy population has been formed at $z = 4.5$. The upper panel shows the predictions of the models $\nu = 3 \text{ Gyr}^{-1}$ (lower curve) and $\nu = 1 \text{ Gyr}^{-1}$ (upper curve), and the lower panel shows the contribution of a 1/2-1/2 mixture of models with $\nu = 1$ and $\nu = 3 \text{ Gyr}^{-1}$. The open circles at low redshift are the measurements from Rao & Turnshek (2000), while the filled circles are the high redshift data from Péroux et al. (2001). Vertical error bars correspond to $1\text{-}\sigma$ uncertainties and the horizontal error bars indicate bin sizes.

of the lines of the $z_{\text{abs}} = 2.625$ DLA toward GB1759+7539 the upper limit $T < 3 \times 10^4 \text{ K}$. In order to assess the choice of an upper temperature limit for the HI gas, Figure 17 shows the evolution of the mass in HI gas, assuming three upper temperature limits ($T \leq 10^4$, 2×10^4 and $3 \times 10^4 \text{ K}$), and also the evolution of the total amount of gas, at any temperature. All the models are run until $t = 13 \text{ Gyr}$. We see that, at late times $t > 1 \text{ Gyr}$, the high temperature gas makes an important contribution to the total gas content of the galaxy. Most of the hot gas is confined to the outer regions of the galaxy ($r \gtrsim 7 \text{ kpc}$) and can achieve temperatures higher than 10^6 K . In a complete census of metal and mass in gas, this hot gas should be included in addition to the HI gas. Figure 17 also shows the evolution of the stellar mass, and of the HI gas fraction with respect to the stellar mass at $z = 0$, assuming a galaxy formation epoch $z_{GF} = 4.5$. The HI gas fraction allows us to relate the HI gas in DLAs to the present day galaxy stellar content. As we see, in the model with $\nu = 1 \text{ Gyr}^{-1}$ the baryonic content is dominated by the total gas at all times, and the stellar mass becomes larger than the HI gas mass only for $t \gtrsim 10 \text{ Gyr}$. By contrast, in the model with $\nu = 3 \text{ Gyr}^{-1}$, the gas is quickly consumed by star formation, and the fraction of HI gas is low during most of the evolution of the model.

Figure 18 shows the evolution of the cosmic HI gas density Ω_g (in units of the critical density) predicted the models with $M_G = 10^9 M_\odot$, and $\nu = 3 \text{ Gyr}^{-1}$ and $\nu = 1 \text{ Gyr}^{-1}$,

compared to the observed Ω_{DLA} evolution. We combine the HI gas fraction calculated from our models with the recent estimate of Ω_m in stars in the local Universe by Cole et al. (2001), $\Omega_*(z=0) = (0.0037 \pm 0.00056)h_{70}^{-1}$. We have assumed that the models are typical of the dwarf galaxy population, and that population was formed at $z_{GF} = 4.5$ and has evolved until $z = 0$, giving rise to the dwarf galaxy contribution to $\Omega_*(z=0)$, i.e. $\Omega_{dwarf} = \Omega_*(M < 0.2M^*) = 0.00098h_{70}^{-1}$, where $M^* = (1.44 \pm 0.37) \times 10^{11}h_{70}^{-2} M_\odot$ is the characteristic mass of the $z = 0$ stellar mass function (Cole et al. 2001). The $\nu = 1 \text{ Gyr}^{-1}$ model is potentially a more important contributor to Ω_{DLA} , due to its larger HI fraction. However, even in the scenario in which each model (with $\nu = 3 \text{ Gyr}^{-1}$ and $\nu = 1 \text{ Gyr}^{-1}$) contributes to a half of Ω_{dwarf} , the dwarf galaxy population can contribute to a half of Ω_{DLA} at $z > 2$, and accounts for nearly all Ω_{DLA} at $z > 3.5$, although at low redshifts its contribution is less important. Therefore, the dwarf galaxies can be an important contributor to Ω_{DLA} , specially at high redshifts.

It is interesting to note that Boissier, Péroux & Pettini (2003), using a family of models for disk galaxies, have found that also the disk galaxies could account for about half of Ω_{DLA} , however, the contribution of the disk population becomes less significant at high redshift, which is the opposite trend of that we find for the dwarf galaxies. This complementarity between the two scenarios, again, argue for a multi-population scenario for DLAs, in which dwarf galaxies are more important at higher redshifts and disks dominate at low redshifts.

5.5 The high redshift cosmic metal content and the relation between DLAs and LBGs

One possible consequence of dust depletion are selection effects in optically selected samples. Boissé et al. (1998) identified a trend of decreasing metallicity with increasing $N(\text{HI})$ for DLAs. They interpreted the lack of systems with large $N(\text{HI})$ and high metallicities as a selection effect due to dust obscuration: systems with large $N(\text{HI})$ and high metallicity (and consequently high dust content) would obscure the background QSO, and would not be selected in an optical survey. This suggestion needs future confirmation, since, in a QSO radio-select survey of DLAs (Ellison et al. 2001b), it was found that the bias due to obscuration of QSOs by the dusty DLAs seems not to be so important.

The presence of dust depletion and possible selection effects rises the question of a possible underestimate of the typical metallicity not only of DLAs but also of other high z systems. Such could be the case of LBGs. The success of the chemodynamical model for spheroids in reproducing the properties of LBGs (Friaça & Terlevich, 1999) gives us confidence in the model prediction that the LBG metal content is easily underestimated from a straightforward interpretation of the observations. The main spectroscopic properties of the LBG population at high z resembles those of star forming galaxies (Steidel et al. 1996b), with spectra characterised by a blue ultraviolet continuum with moderate dust extinction, strong interstellar absorption, P Cygni CIV and NV lines from massive stars, and weak Lyman α emission (Lowenthal et al. 1997, Pettini et al. 1998, 2000b). Although the LBGs are very important objects in the study of the chemical enrichment of the early universe because they are

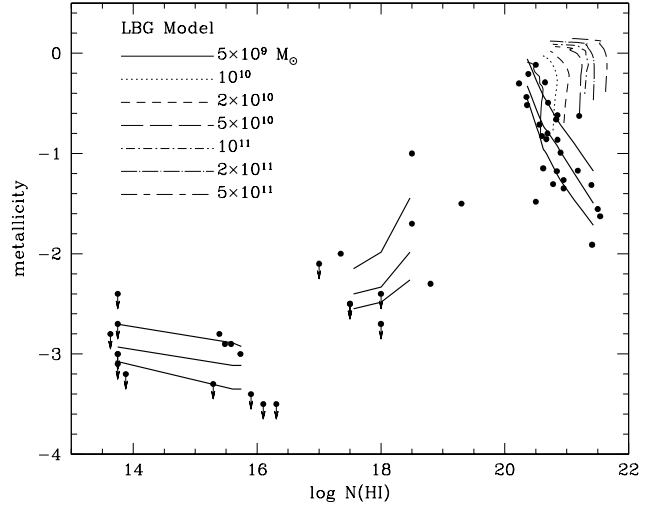


Figure 19. Metallicity vs. $N(\text{HI})$ data for several classes of high z objects: LAF clouds, LLSs and DLAs, in order of increasing $N(\text{HI})$. For DLAs, the metallicity is given by $[\text{Si}/\text{H}]_{\text{cor}}$ derived in this paper, and, for LLS and LAF, it is given by $[\text{O}/\text{H}]$, estimated from the observed $[\text{C}/\text{H}]$ (LAF data taken from Lu 1991 and Lu et al. 1998a, and LLS data from Steidel 1990) assuming $[\text{O}/\text{C}] = 0.3$ (Viegas et al. 1999). The curves in the right-upper corner are the predictions for LBGs from chemodynamical models with several masses, and the metallicity is $[\text{O}/\text{H}]$, averaged over a 10 kpc projected radius; the evolution is shown from 0.1 Gyr (lowest point of the curve) until 1 Gyr. The thick solid lines are the statistical fits to the data.

the most obvious star forming regions at high z , they are not suited for chemical abundance studies. Despite the high quality of their spectra, the large equivalent width of the saturated interstellar lines and the high velocity dispersions in the ISM of these galaxies make abundance determination in LBGs difficult. However, combining observational data and modelling allows one to infer typical LBG metallicities in the range of $0.3 Z_\odot$ to Z_\odot (Friaça & Terlevich 1999).

Another question is whether DLAs are related to the LBGs. Mo et al. (1999) proposed that LBGs and DLAs form distinct populations: the LBGs would be star forming galaxies with low angular momentum and short collapse time scale, while the DLAs would be the initial stages of evolution of galaxies with high angular momentum and longer collapse times.

In order to investigate these questions, Figure 19 compares metallicity vs. $N(\text{HI})$ trends obtained in this work for DLAs not only to predictions of the chemodynamical model for LBGs (Friaça & Terlevich 1999), but also to data of Ly α forest (LAF) clouds and LLSs. As we see from Figure 19, the most metal-rich DLAs could be $M_G \lesssim 10^{11} M_\odot$ LBGs in their early evolutionary phases (the $10^{11} M_\odot$ model is the progenitor of a present-day $\sim 0.3 L^*$ spheroid), but most of DLAs are not explained as LBGs. The LBGs typically are sub- L^* systems: the characteristic velocity dispersion of the emission lines, $\sigma_{em} \approx 70 \text{ km}^{-1}$ (Pettini et al. 1998; Pettini et al. 2001), is reproduced by $M_G \approx 10^{10} M_\odot$ models (Friaça & Terlevich 1999). However, it seems that most of the DLA galaxies would be still fainter than the spectroscopically detected LBGs. Good fits to the abundance data are obtained for the $\approx 10^9 M_\odot$ model.

It is interesting to note that other lines of evidence point toward to masses not far from $\sim 10^9 M_{\odot}$ as typical for DLAs. A recent Arecibo blind 21 cm survey (Rosenberg & Schneider 2003) has revealed that the number of systems per unit redshift is dominated by galaxies with HI masses near $10^9 M_{\odot}$. Zheng & Miralda-Escudé (2002) modelled DLAs as spherical isothermal gaseous halos ionized by the extragalactic ionizing background, and concluded that self-shielding implies a DLA HI mass of $\approx 1.6 \times 10^8 M_{\odot}$ for $N(\text{HI}) \approx 3 \times 10^{20} \text{ cm}^{-2}$.

Notice that the normalization of the star formation rate for the LBG models is $\nu = 10 \text{ Gyr}^{-1}$, whereas for the DLA models shown in this paper, $\nu = 3$ or 1 Gyr^{-1} . The star formation proceeds slowly in DLAs, which would give support to the scenario for galaxy formation in which there is a dichotomy between the star formation modes for DLAs (long star formation time scale) and LBGs (short star formation time scale). However, the star formation in DLAs does not need to be much different from that of typical LBGs, since a normalization of the SFR only a factor ~ 3 smaller accounts the properties of a number of DLAs, thus allowing for a smoother progression in the evolutionary history of DLAs and LBGs rather than a sharp dichotomy between the two populations (see Møller et al. 2002).

A complete analysis of the metallicity vs. $N(\text{HI})$ relation for DLAs should take into account the evolution of metallicity with the redshift, and the fact that this evolution depends on the column density, and, in particular, that no evolution with redshift is observed at $\log N(\text{HI}) > 21$ (Boissé et al. 1998, Savaglio 2000). On the other hand, for systems with low column densities, $\log N(\text{HI}) < 20.8$, the metallicity does decrease with the redshift (Savaglio 2000). In any case, the gaps in Figure 19 highlight domains in column density for which further investigation is required. There is some suggestion of underestimate of the metal content in DLAs from the fact that near $\log(N(\text{HI})) \approx 20.5$, there seems to be a smooth transition between LBGs and DLAs, whereas at higher HI column densities, there is a gap between the two classes of objects. It is possible that a whole class of objects, intermediate between the observed DLAs and LBGs, are missing at $\log(N(\text{HI})) \gtrsim 21$. These could be high metallicity dusty DLA-like objects or LBG-like objects that are too faint or have too red $G - \mathcal{R}$ colours to be classified as LBGs. Also on the low $N(\text{HI})$ side of the DLA distribution it is possible to hide significant amounts of metal. The trend of increasing metallicity with decreasing $N(\text{HI})$ extends down to the lowest values of $N(\text{HI})$ accepted for DLAs ($\log(N(\text{HI})) \approx 20$), and then there is a new gap, filled with a few LLSs and sub-DLAs. This gap suggests that a large number of these objects is missing. In addition, the ionization corrections for these systems are very complex, and their chemical abundances easily could be underestimated. Proper consideration of the radiation fields and adequate application of photoionization codes could lead to metallicity estimates for some LLSs in the range of $0.1 Z_{\odot}$ to Z_{\odot} (Viegas & Friaça 1995). The ionization corrections should include high ions, which can make a sizeable contribution to the total metal column density, specially if we take into account that, as said in Section 4.3, these systems are preferentially located in the outer regions of the galaxy, where the hot gas concentrates and gives rise to a local EUV/soft X-ray ionizing radiation field (Viegas & Friaça 1995, Viegas

et al. 1999). In this sense, the data points of LLSs in Figure 19 may represent lower limits to the actual metallicities of these systems. Therefore, these low column density systems might represent important reservoirs of metals at high redshifts (see Péroux et al. 2001). If we are missing important populations of chemically evolved objects, the overall metal content in the Universe at high redshift has been underestimated, in this way alleviating somewhat the problem that the density of metal detected at high redshift is smaller than the integrated total metal production associated with the star formation activity at high-redshift (Pettini 2000, Pagel 2000).

6 SUMMARY AND CONCLUSIONS

In this paper we have explored several scenarios for the nature of the DLAs by means of a study of the metallicity evolution of these systems. We have analysed the observational data on chemical abundances of DLAs with robust statistical methods, and corrected the abundances for dust depletion. The results of this analysis have been compared to predictions of several classes of chemical evolution models describing a variety of scenarios for DLAs: one-zone dwarf galaxy models, multi-zone disk models, and chemodynamical models representing dwarf galaxies. We have found that the chemodynamical model for dwarf galaxies is more successful than our dwarf galaxy one-zone models and the disk models in reproducing the properties — abundances, abundance ratios, and HI and metal column densities — of DLAs. We have then focused on the dwarf galaxy scenario for DLAs, as described by the chemodynamical model, and investigated a number of issues: the epoch of formation of the host galaxies of DLAs, the contribution of dwarf galaxies to Ω_{DLA} , the multi-population (disks and dwarf galaxies) scenario for DLAs, the relation of DLAs and LBGs, possible missing populations of high redshift objects, and “hidden” reservoirs of metals at high redshifts. We summarise our results as follows.

1) The α -enhancement observed in DLAs seems to be real, even after dust corrections have been applied to the data. In our sample, the observed $[\text{Si}/\text{Fe}]_{\text{median}} = 0.32$ is lowered to $[\text{Si}/\text{Fe}]_{\text{median}} = 0.16$ by the dust correction, but remains typically suprasolar, a pattern similar to that found in metal-poor stars of the Galactic disk. However, there are DLAs with nearly solar $[\text{Si}/\text{Fe}]$ ratio even at low metallicities, which could be hosted by dwarf galaxies instead of by disks.

2) The bimodality in the $[\text{N}/\alpha]$ vs. $[\alpha/\text{H}]$ distribution of DLAs pointed out by Prochaska et al. (2002b) is less apparent in our sample. Instead we find a lower bound envelope in the $[\text{N}/\alpha]$ vs. $[\alpha/\text{H}]$ distribution, above which the DLAs are concentrated, and that corresponds to a local specific star formation rate $\nu \approx 3 \text{ Gyr}^{-1}$. This envelope is close to the evolutionary tracks of the one-zone dwarf galaxy model with $\nu = 3 \text{ Gyr}^{-1}$, and of the disk model at $r = 4 \text{ kpc}$, but its shape is best reproduced by the dwarf galaxy chemodynamical model at $r = 1 \text{ kpc}$.

3) The one-zone models, both for disk systems and dwarf galaxies, present an apparent discrepancy between fits using $[\text{Si}/\text{Fe}]$ and $[\text{N}/\alpha]$ ratios. In the disk model, the $[\text{Si}/\text{Fe}]$ ratios are better reproduced in larger radii than those re-

quired by the $[N/\alpha]$ ratios, and, in the dwarf galaxy model, by lower values of ν than those implied by the $[N/\alpha]$ ratios.

4) The chemodynamical model for dwarf galaxies is more successful than the pure chemical evolution models in reproducing the properties in DLAs. The connection between the gas flow evolution and the star formation rate is the reason behind this ability of the chemodynamical model. The chemodynamical model presents multiple star bursts, fed by gas flows which lead the evolutionary tracks of the model to cover all the values exhibited by the $[Si/Fe]$ vs. $[Fe/H]$ and $[N/\alpha]$ vs. $[\alpha/H]$ distributions of the DLAs. A multi-burst model for DLAs have already be proposed by Matteucci et al. (1997), but, in the chemodynamical model, the starbursts appear in a natural way, with no need of additional parameters describing them.

5) From the study of DLAs with simultaneous measurements of $[N/\alpha]$ and $[\alpha/Fe]$ ratios we have inferred the ages and formation epoch z_{GF} of DLAs. We have found that $z_{GF} = 1.7 - 4.5$, and ages ranging from 0.1 Gyr to 1 Gyr. Higher values of z_{GF} could be achieved if we consider the systems with highest values of $[Fe/H]$, supposed to be the most chemically evolved, and good candidates to be old systems. In this case, we find $z_{GF} \sim 3 - 8$. One general conclusion is that DLAs constitute a relatively young population with ages not exceeding 2 Gyr, or even 1 Gyr.

6) The dwarf galaxies can contribute to about half of Ω_{DLA} at $z > 2$, and even more, at $z > 3.5$, although at low redshifts their contribution is less important. A multi-population scenario for DLAs seems to favoured, in which the DLA population is dominated by dwarf galaxies at high redshifts and by disks at lower redshifts.

7) The results of the chemodynamical model calls for a smoother progression in the evolutionary history of DLAs and LBGs rather than a sharp dichotomy between the two populations. LBGs and DLAs could constitute a sequence of increasing star formation rate, with the LBGs being the systems with typically short star formation time scales ($\sim 10^8$ yr), and the DLAs corresponding to the low ν ($\approx 1 - 3$ Gyr $^{-1}$) end of the sequence. We also arise the possibility that we could be missing a whole population of objects at high hydrogen density columns with metallicities intermediate between those of DLAs and LBGs.

8) It is possible that relying only on the observations of DLAs could lead to an underestimate of the metal content of the high redshift Universe, because we are not properly including in the metal census both the above mentioned high column density population and the low column density population constituted by LLSs and sub-DLAs.

ACKNOWLEDGMENTS

We thank Timothy Beers for making available the *LOWESS* and *MSTAT* routines to us and for the help with the robust statistical methods. We thank the anonymous referee for the detailed comments which improved this work. G.A.L. and A.C.S.F. acknowledge financial support from the Brazilian agencies CNPq, FAPESP (proj. 00/10972-0) and CNPq/PRONEX.

REFERENCES

- Archibald E. N., Jimenez R., Dunlop J.S., Friaça, A. C. S., McLure R.J., Hughes D.H., 2002, MNRAS, 336, 353
 Bender R., Burstein D., Faber S.M., 1993, ApJ, 411, 153
 Boissé P., Le Brun V., Bergeron J., Deharveng J.M., 1998, A&A, 333, 841
 Boissier S., Prantzos N., 2000, MNRAS, 312, 398
 Boissier S., Péroux C., Pettini M., 2003, MNRAS, 338, 131
 Bowen D.V., Tripp T.M., Jenkins E.B., 2001, AJ, 121, 1456
 Calura F., Matteucci F., Vladilo G., 2002, astro-ph/0211153
 Carretta E., Gratton R., Cohen J.G., Beers T.C., Christlieb N., 2002, AJ, 124, 481.
 Cen R., Ostriker J.P., Prochaska J.X., Wolfe A.M., 2002, astro-ph/0203524
 Centurión M., Bonifacio P., Molaro P., Vladilo G., 2000, ApJ, 536, 540
 Centurión M., Molaro P., Vladilo G., Péroux C., Levshakov A., D’Odorico V., 2003, astro-ph/0302032
 Chiappini C., Matteucci F., Gratton R., 1997, ApJ, 477, 765
 Cleveland W.S., Devlin S.J., 1988, J. Am. Stat. Assoc., 83, 596
 Cleveland W.S., Kleiner B., 1975, *Technometrics*, 17, 447
 Cole S., et al., 2001, MNRAS, 326, 255
 Cowie L.L., Songaila A., Kim, T., Hu E.M., 1995, AJ, 109, 1522
 Dessauges-Zavadsky M., D’Odorico S., McMahon R.G., Molaro P., Ledoux C., Péroux C., Storrie-Lombardi L.J., 2001, A&A, 370, 426
 Dessauges-Zavadsky M., Prochaska J.X., D’Odorico S., 2002, A&A, 391, 801
 Diaz A.J., 1980, in Beckman J.E., Pagel B.E.J., eds, *Evolutionary Phenomena in Galaxies*. CUP, Cambridge, p. 377
 Ellison S.L., Lopez S., 2001, A&A, 380, 117
 Ellison S.L., Lopez S., 2002, A&A, 392, 489
 Ellison S.L., Pettini M., Steidel C.C., Shapley A.E., 2001a, ApJ, 549, 770
 Ellison S.L., Yan L., Hook I.M., Pettini M., Wall J.V., Shaver P., 2001b, A&A, 379, 393
 Friaça A.C.S., 2000, in Trinh Y.T., Balkowski C., Cayatte V., Ván J.T.T., eds, *Dwarf Galaxies and Cosmology*. Editions Frontières, Paris, p.312
 Friaça A.C.S., 1993, A&A, 269, 145
 Friaça A.C.S., Jafelice L.C., 1999, MNRAS, 302, 491
 Friaça A.C.S., Terlevich R.J., 1998, MNRAS, 298, 399
 Friaça A.C.S., Terlevich R.J., 1999, MNRAS, 305, 90
 Friaça A.C.S., Terlevich R.J., 2001, MNRAS, 325, 335
 Gonçalves D.R., Friaça A.C.S., 1999, MNRAS, 309, 651
 Grevesse N., Sauval A.J., 1998, *Space Science Reviews*, 85, 161
 Haehnelt, M., Steinmetz, M. & Rauch, M., 1998, ApJ, 495, 647
 Holweger H., 2001, in Wimmer-Schweingruber R.F., ed., *Solar and Galactic Composition*. Springer, Berlin, p.23
 Hou J.L., Boissier S., Prantzos N., 2001, A&A, 370, 23
 Iwamoto K., Brachwitz F., Nomoto K., Kishimoto N., Umeda H., Hix W.R., Thielemann F.-K., 1999, ApJS, 125, 439
 Izotov Y.I., Thuan T.X., 1999, ApJ, 511, 639
 Izotov Y.I., Schaerer D., Charbonnel C., 2001, ApJ, 549, 878
 Jimenez R., Friaça, A. C. S, Dunlop J.S., Terlevich, R. J., Peacock J.A., & Nolan L.A., 1999, MNRAS, 305, L16
 Johnson, J.A., 1999, PhD thesis, UC Santa Cruz
 Kauffmann G., 1996, MNRAS, 281, 75
 Kauffmann, G. & Haehnelt, M. 2000, MNRAS, 311, 576
 Larson R.B., 1974, MNRAS, 169, 229
 Lauroesch J.T., Truran J.W., Welty D.E., York D.G., 1996, PASP, 108, 641
 Le Brun V., Bergeron J., Boissé P., Deharveng J. M., 1997, A&A, 321, 733
 Ledoux C., Petitjean P., Bergeron J., Wampler E.J., Srianand R., 1998, A&A, 337, 51
 Ledoux C., Srianand R., Petitjean P., 2002, A&A, 392, 781

- Levshakov S.A., Dessauges-Zavadsky M., D'Odorico S., Molaro P., 2002, *ApJ*, 565, 696
- Loewestein M., Mushotzky R.F., 1996, *AJ*, 466, 695
- Lopez S., Reimers D., Rauch M., Sargent W.L.W., Smete A., 1999, *ApJ*, 513, 598
- Lopez S., Reimers D., D'Odorico S., Prochaska J.X., 2002, *A&A*, 385, 778
- Lowenthal J. et al. 1997, *ApJ*, 481, 673
- Lu L., 1991, *ApJ*, 379, 99
- Lu L., Sargent W.L.W., Barlow T.A., Churchill C.W., Vogt S., 1996, *ApJS*, 107, 475
- Lu L., Sargent W.L.W., Barlow T.A., Rauch M., 1998a, *astro-ph/9802189*
- Lu L., Sargent W.L.W., Barlow T.A., 1998b, *AJ*, 115, 55
- Matteucci F., 1994, *A&A*, 288, 57
- Matteucci F., François P., 1989, *MNRAS*, 239, 885
- Matteucci F., Tornambé A., 1987, *A&A*, 185, 51
- Matteucci F., Molaro P., Vladilo G., 1997, *AAp*, 321, 45
- Mo, H.J., Mao, S., White, S.D.M., 1999, *MNRAS*, 304, 17
- Molaro P., D'Odorico S., Fontana A., Savaglio S., Vladilo G., 1996, *AAp*, 308, 1
- Molaro P., Levshakov S.A., D'Odorico S., Bonifacio P., Centurión M., 2001, *ApJ*, 549, 90
- Møller P., Warren S.J., Fall S.M., Fynbo J.U., Jakobsen P., 2002, *ApJ*, 574, 51
- Nagamine K., Springel V., Hernquist L., 2003, *astro-ph/0302187*
- Pagel B.E.J., 1999, *astro-ph/9911204*
- Pei Y., Fall S., 1995, *ApJ*, 454, 69
- Péroux C., Irwin M.J., McMahon R.G., Storrie-Lombardi L.J., 2001, *astro-ph/0107045*
- Péroux C., Irwin M.J., McMahon R.G., Storrie-Lombardi L.J., 2002a, in Fusco-Fermiano R., Matteucci F., eds, *Chemical Enrichment of the Intracluster and Intergalactic Medium*, *PASP Conf. Proc.* 253. ASP, San Francisco, p. 501
- Péroux C., Petitjean P., Aracil B., Srianand R., 2002b, *NewA*, 7, 577
- Petitjean P., Srianand R., Ledoux C., 2002, *MNRAS*, 392, 781
- Pettini M., 1999, in Walsh J.R., Rosa M.R., eds, *Chemical Evolution from Zero to High Redshift*. Springer-Verlag, Berlin, p. 233
- Pettini M., 2000, *Phil. Trans. R. Soc. Lond. A*, 358, 2035
- Pettini M., Smith L.J., Hunstead R.W., King D.L., 1994, *ApJ*, 426, 79
- Pettini M., King D.L., Smith L.J., Hunstead R.W., 1997a, *ApJ*, 478, 536
- Pettini M., Smith L.J., King D.L., Hunstead R.W., 1997b, *ApJ*, 486, 665
- Pettini M., Kellog M., Steidel C.C., Dickinson M.E., Adelberger K.L., Giavalisco M., 1998, *ApJ*, 508, 539
- Pettini M., Ellison S.L., Steidel C.C., Bowen D.V., 1999, *ApJ*, 510, 576
- Pettini M., Ellison S.L., Steidel C.C., Shapley A. E., Bowen D.V., 2000a, *ApJ*, 532, 65
- Pettini M., Steidel C.C., Adelberger K.L., Dickinson M.E., Giavalisco M., 2000b, *ApJ*, 528, 96
- Pettini M., Shapley A. E., Steidel C.C., Cuby J.-G., Dickinson M.E., Moorwood A.F.M., Adelberger K.L., Giavalisco M., 2001, *ApJ*, 554, 981
- Pettini M., Ellison S.L., Bergeron J., Petitjean P., 2002, *A&A*, 391, 21
- Prantzos N., Boissier S., 2000, *MNRAS*, 315, 82
- Prochaska J.X., Wolfe A.M., 1997, *ApJ*, 474, 140
- Prochaska J.X., Wolfe A.M., 1998, *ApJ*, 507, 113
- Prochaska J.X., Wolfe A.M., 1999, *ApJS*, 121, 369
- Prochaska J.X., Wolfe A.M., 2002, *ApJ*, 566, 68
- Prochaska J.X., Naumov S.O., Carney B.W., McWilliam A., Wolfe A.M., 2000, *AJ*, 120, 2513
- Prochaska J.X., Wolfe A.M., Tytler D., Burles S., Cooke J., Gawiser E., Kirkman D., O'Meara J.M., Storrie-Lombardi L., 2001, *ApJS*, 137, 21
- Prochaska J.X., Howk J.C., O'Meara J.M., Tytler D., Wolfe A.M., Kirkman D., Lubin D., Suzuki N., 2002a, *ApJ*, 571, 693
- Prochaska J.X., Henry R.B.C., O'Meara J.M., Tytler D., Wolfe A.M., Kirkman D., Lubin D., Suzuki N., 2002b, *PASP*, 114, 933
- Rao S., Turnshek D.A., 2000, *ApJS*, 130, 1
- Ryan S.G., Norris J.E., Beers T.C., 1996, *ApJ*, 471, 254
- Rosenberg J.L., Schneider S.E., 2003, *ApJ*, 585, 256
- Roth K.C., Blades J.C., 1995, *ApJ*, 445, 95
- Salpeter E. E., 1955, *ApJ*, 121, 161
- Sargent W.L.W., Young P., Boksenberg A., Tytler D., 1980, *ApJS*, 42, 41
- Savage B.D., Sembach K.R., 1996, *Ann. Rev. Astron. Astrophys.*, 34, 279
- Savaglio S., 2001, in Harwit M., Michael G. Hauser M.G., eds, *The extragalactic infrared background and its cosmological implications*, *ASP Conf. Ser.* 204. Astron. Soc. Pac., San Francisco, p. 307
- Savaglio S., Panagia N., Stiavelli M., 2000, in Franco J., Terlevich L., López-Cruz O., Aretxaga I, eds, *Cosmic Evolution and Galaxy Formation*, *ASP Conf. Ser.* 215. Astron. Soc. Pac., San Francisco, p. 65
- Sembach K.R., Savage B.D., 1996, *ApJ*, 457, 211
- Schaye J., 2001, *ApJ*, 562, L95
- Snedden C., Gratton R.G., Crocker D.A. 1991, *A & A*, 246, 354
- Somerville, R., Primack, J. & Faber, S., 2000, *MNRAS*, 320, 504
- Songaila A., Cowie L.L., 1996, *AJ*, 112, 335
- Steidel C.C., 1990, *ApJS*, 74, 37
- Steidel C.C., Giavalisco M., Dickinson M.E., Adelberger K.L., 1996a, *AJ*, 112, 352
- Steidel C.C., Giavalisco M., Pettini M., Dickinson M.E., Adelberger K.L., 1996b, *ApJ*, 462, L17
- Storrie-Lombardi L.J., Wolfe A.M., 2000, *ApJ*, 543, 552
- Timmes F.X., Woosley S.E., Weaver T.A., 1995, *ApJS*, 98, 617
- Tytler D., 1982, *Nat*, 298, 427
- Turnshek D.A. Rao S., Nestor D., Lane W., Monier E., Bergeron J., Smette A., 2001, *ApJ*, 553, 288
- Umeda H., Nomoto K., 2002, *ApJ* 565, 385
- van de Hoek L.B., Groenewegen M.A.T., 1997, *A&A*, 123, 305
- Van Zee L., Haynes P.M., Salzer J.J., 1997a, *AJ*, 114, 2479
- Van Zee L., Haynes P.M., Salzer J.J., 1997b, *AJ*, 114, 2497
- Viegas S. M., 1995, *MNRAS*, 276, 268
- Viegas S. M., Friaça A. C. S., 1995, *MNRAS*, 272, L35
- Viegas S. M., Friaça A. C. S., Gruenwald R., 1999, *MNRAS*, 309, 355
- Viegas S. M., Gruenwald R., 1991, *ApJ*, 377, 39
- Vladilo G., 1998, *ApJ*, 493, 583
- Vladilo G., 2002a, *ApJ*, 569, 295
- Vladilo G., 2002b, *A&A*, 391, 407
- Vladilo G., Centurión M., Bonifacio P., Howk J.C., 2001, *ApJ*, 557, 1007
- Wolfe A.M., Prochaska J.X., 2000a, *ApJ*, 545, 591
- Wolfe A.M., Prochaska J.X., 2000b, *ApJ*, 545, 603
- Wolfe A.M., Turnshek D.A., Smith H.E., Cohen R.D., 1986, *ApJS*, 61, 249
- Wolfe A.M., Lanzetta K.M., Foltz C.B., Chaffee F.H., 1995, *ApJ* 454, 698
- Woosley S.E., Weaver T.A., 1995, *ApJS*, 101, 181
- Zheng Z., Miralda-Scudé J., 2002, *ApJ*, 568, L71

This paper has been produced using the Royal Astronomical Society/Blackwell Science \LaTeX style file.